Gastrointestinal involvement attenuates COVID-19 severity and mortality

Authors: Alexandra E. Livanos[1,2]*, Divya Jha[1,2]*, Francesca Cossarini[1,3]*, Ana S. Gonzalez-Reiche[4]* Minami Tokuyama[1,2]*, Teresa Aydillo[5,15]*, Tommaso L. Parigi[6]*, Irene Ramos[7], Katie Dunleavy[8], Brian Lee[9], Rebekah Dixon[2], Steven T. Chen[1,10], Gustavo Martinez-Delgado[1,2], Satish Nagula[2], Huaibin M. Ko[2,11], Jason Reidy[11], Steven Naymagon[2], Ari Grinspan[2], Jawad Ahmad[2], Michael Tankelevich[1,2], Ronald Gordon[11], Keshav Sharma[1,2], Graham J. Britton[1,12], Alice Chen-Liaw[1,12], Matthew P. Spindler[1,12], Tamar Plitt[1,12], Pei Wang[4], Andrea Cerutti[1,13,14], Jeremiah J. Faith[1,12], Jean-Frederic Colombel[1,2], Ephraim Kenigsberg[1,4], Carmen Argmann[4], Miriam Merad[1,8,9,10], Sacha Gnjatic[1,8,9,10,11], Noam Harpaz[11], Silvio Danese[6], Adeeb Rahman[1,4,9,10], Nikhil A. Kumta[2], Alessio Aghemo[6], Francesca Petralia[4†], Harm van Bakel[4,12†], Adolfo Garcia-Sastre[3,5,15†] and Saurabh Mehandru[1,2†]

* These authors contributed equally to this work.
† These authors contributed equally to this work.

Please address correspondence to:
saurabh.mehandru@mssm.edu,
adolfo.Garcia-Sastre@mssm.edu,
harm.vanbakel@mssm.edu, or
francesca.Petralia@mssm.edu

Authors affiliations

[1]Precision Immunology Institute, Icahn School of Medicine at Mount Sinai, New York, NY 10029
[2]The Dr. Henry D. Janowitz Division of Gastroenterology, Department of Medicine, Icahn School of Medicine at Mount Sinai, New York, NY 10029
[3]Division of Infectious Disease, Department of Medicine, Icahn School of Medicine at Mount Sinai, New York, NY 10029
[4]Department of Genetics and Genomic Sciences, Icahn School of Medicine at Mount Sinai, New York, NY 10029, USA.
[5]Department of Microbiology, Icahn School of Medicine at Mount Sinai, New York, NY 10029
[6]Department of Biomedical Sciences, Humanitas University, Milan, Italy.
[7]Department of Neurology and Center for Advanced Research on Diagnostic Assays, Icahn School of Medicine at Mount Sinai, New York, New York, 10029.
[8]Department of Medicine, Icahn School of Medicine at Mount Sinai, New York, NY 10029
[9]Human Immune Monitoring Center (HIMC) Icahn School of Medicine at Mount Sinai New York, New York, 10029
[10]Department of Oncological Sciences, Icahn School of Medicine at Mount Sinai, New York, NY, USA
[11]Department of Pathology, Icahn School of Medicine at Mount Sinai, New York, NY 10029
[12]Icahn Institute for Data Science and Genomic Technology, Icahn School of Medicine at Mount Sinai, New York, NY, 10029
[13]Catalan Institute for Research and Advanced Studies (ICREA), Barcelona, Spain
[14]Program for Inflammatory and Cardiovascular Disorders, Institut Hospital del Mar d'Investigacions Mèdiques (IMIM), Barcelona, Spain
[15]Global Health and Emerging Pathogens Institute, Icahn School of Medicine at Mount Sinai, New York, NY, USA.

A.E.L.: Gastroenterology Fellow, D.J.: Postdoctoral Fellow, F.C.: Assistant Professor, A.S.G-R.: Postdoctoral Fellow, M.T.: MD candidate, T.A.: Instructor, T.L.P.: Gastroenterology Fellow, I.R.: Assistant Professor, K.D.: Internal Medicine Resident, B.L.: Computational Scientist , R.D.: Senior Research Coordinator, S.T.C.: MD/PhD candidate, G.M.D.: Research manager, S.N.: Associate Professor, H.M.K.: Assistant Professor, J.R.: Electron Microscopist, S.N.: Assistant Professor, A.G.: Assistant Professor, J.A.: Professor, M.T.: Research Coordinator, R.G.: Research Professor, K.S.: Master's candidate, G.J.B.: Instructor, A.C.L.: MD/PhD candidate, M.P.S.: MD/PhD candidate, T.P.: PhD candidate, P.W.: Professor, A.C.: Professor, J.J.F.: Associate Professor, J.F.C.: Professor, E.K.: Assistant Professor, C.A.: Associate Professor, M.M.: Professor, S.G.: Associate Professor, N.H.: Professor, S.D.: Professor, A.R.: Associate Professor, N.A.K.: Associate Professor, A.A.: Associate Professor, F.P.: Assistant Professor, H.V.B.: Assistant Professor, A.G.S.: Professor, S.M.: Associate Professor.

Abstract

Given that gastrointestinal (GI) symptoms are a prominent extrapulmonary manifestation of coronavirus disease 2019 (COVID-19), we investigated the impact of GI infection on disease pathogenesis in three large cohorts of patients in the United States and Europe. Unexpectedly, we observed that GI involvement was associated with a significant reduction in disease severity and mortality, with an accompanying reduction in key inflammatory proteins including IL-6, CXCL8, IL-17A and CCL28 in circulation. In a fourth cohort of COVID-19 patients in which GI biopsies were obtained, we identified severe acute respiratory syndrome coronavirus-2 (SARS-CoV-2) within small intestinal enterocytes for the first time *in vivo* but failed to obtain culturable virus. High dimensional analyses of GI tissues confirmed low levels of cellular inflammation in the GI lamina propria and an active downregulation of key inflammatory genes including *IFNG*, *CXCL8*, *CXCL2* and *IL1B* among others. These data draw attention to organ-level heterogeneity in disease pathogenesis and highlight the role of the GI tract in attenuating SARS-CoV-2-associated inflammation with related mortality benefit.

Introduction

Coronavirus disease 2019 (COVID-19), is a multisystem illness caused by severe acute respiratory syndrome coronavirus 2 (SARS-CoV-2) a recently discovered novel betacoronavirus[1-3]. Manifestations of COVID-19 range from asymptomatic infection to severe, life-threatening disease with end-organ damage[3-5]. Common symptoms of COVID-19 include fever, cough, and shortness of breath that occur within 2 to 14 days after exposure to SARS-CoV-2[6]. A subset of COVID-19 patients also report gastrointestinal (GI) symptoms, comprising nausea, vomiting, diarrhea, abdominal pain and/or loss of appetite[7-11], which is not surprising given that the host receptor for SARS-CoV-2 (ACE2 receptor) is highly expressed on intestinal epithelium[12,13]. Several studies have demonstrated the presence of SARS-CoV-2 RNA in the fecal samples of infected persons[11,14-17] and in some cases even after clearance from respiratory samples[17]. Additionally, several members of the *Coronaviridae* family are known to be enterotropic, causing gastroenteritis in addition to respiratory illness[18]. Notably, SARS-CoV and MERS-CoV, closely related to SARS-CoV-2, have been identified in fecal samples of infected individuals[19-22]. Finally, the presence of GI involvement by SARS-CoV-2 has also been suggested by epidemiological[23], clinical[24], non-human primate[25] and *in vitro*[26-29] data. However, to date there is no evidence of SARS-CoV-2 infection of human enterocytes *in vivo* and there are no studies on the responses of the GI immune system, arguably the largest in the body, in COVID-19 patients.

Immune dysregulation has been suggested as a primary driver of morbidity and mortality in COVID-19. Several cytokines and other immunological parameters have been correlated with COVID-19 severity. Most notably, elevated IL-6, IL-8, IL-10, MCP-1 and IP-10 levels were detected in hospitalized patients, especially critically ill patients, in several studies, and are associated with ICU admission, respiratory failure, and poor prognosis[3,30-36]. Alongside this pro-inflammatory cytokine environment, significant immune cell alterations have been described such as lymphopenia, T and B cell activation and exhaustion[37], as well as altered frequencies of myeloid cells, including conventional dendritic cells (cDCs) and plasmacytoid dendritic cells (pDCs)[5,38,39].

Given the emerging evidence of enteric involvement by SARS-CoV-2, immune dysregulation in COVID-19 and the propensity of the GI immune system to suppress inflammation, we aimed to define the role of the GI tract in the pathogenesis of COVID-19. Here, we present findings on four well-characterized cohorts of COVID-19 patients hospitalized in tertiary care centers in New York City, USA and Milan, Italy, where we conducted high dimensional analyses of mucosal and systemic immune parameters and investigated disease outcomes associated with GI involvement in COVID-19 patients.

Results

Clinical characteristics of discovery cohort

We initiated a large, multi-cohort study to determine the role of the GI tract in the pathogenesis of SARS-CoV-2 infection. Our initial, 'discovery cohort' comprised 925 patients who tested PCR positive for SARS-COV-2 at the Mount Sinai Hospital (MSH) in New York City between April 1, 2020 and April 15, 2020. Among these 925 patients, 634 cases met our inclusion criteria of hospital admission, age > 18 years and having a multiplexed cytokine panel performed during their admission (**Supplementary Fig. 1**). The basic demographics and clinical characteristics are summarized in **Table 1**. Patients were 64 ± 16 years old (range 23-99 years) with 369 (58%) of the patients being male. The cohort comprised 28% Hispanic, 25% African American, 22% White and the remainder Asian or other based on patient's self-reported ethnicity. Comorbid illnesses included obesity (37%), hypertension (HTN) (36%) and diabetes mellitus (DM) (22%), similar to prior reports[40]. Fifty-four (9%) patients had mild disease, 361 (57%) moderate, 158 (25%) severe and 61 (10%) had severe COVID-19 with end organ damage (EOD) (**Table 2**, disease severity defined in Methods and **Supplementary Table 1**). During hospitalization, 110 patients were admitted to the ICU (17%) and 151 patients (24%) died by the end of data collection (6/15/2020) (**Table 2**).

We analyzed diarrhea, nausea and vomiting at the time of hospital admission. Two hundred and ninety-nine patients (47%) reported any GI symptoms (nausea, vomiting and/or diarrhea) with diarrhea being the most common (245 patients, 39%), followed by nausea (157 patients, 25%), and then vomiting (82 patients, 13%) (**Table 3**). Patients with GI symptoms were significantly younger (average age 61 years) than those without GI symptoms (average age 67 years) ($p<0.0001$) (**Table 1**). The distribution of race, ethnicity and co-morbid illnesses including obesity, HTN, DM and inflammatory bowel diseases (IBD) were comparable between those with GI symptoms and those without GI symptoms (**Table 1**).

COVID-19 severity was significantly reduced in patients with GI symptoms when compared to those without GI symptoms

In an effort to determine the association between GI symptoms and COVID-19 severity, we initially performed univariate analysis comparing the distribution of COVID-19 severities in patients with and without GI symptoms. Patients presenting with GI symptoms had less severe disease than patients without GI symptoms ($p<0.001$ Chi-square test). Importantly, mortality was significantly lower in COVID-19 patients with GI symptoms (15.7%) than those without GI symptoms (31.0%; $p<0.0001$ Fisher's exact test) (**Table 2, Fig. 1a**). Furthermore, each individual GI symptom

188 (nausea, vomiting and diarrhea) was associated with less severe disease ($p<0.02$ Fisher's exact
189 test) and lower mortality ($p<0.001$ Fisher's exact test) (**Fig. 1a**). These findings were further
190 emphasized by Kaplan-Meier estimates of survival over short-term follow-up of 25 days ($p<0.001$
191 log-rank test) (**Fig. 1b, Supplementary Fig. 2a**). Consistent with prior reports[35,40,41] older age and
192 higher disease severity were associated with higher mortality in the discovery cohort (**Table 4**),
193 providing validity to our findings.
194 Next, we decided to account for multiple comorbidities in determining the impact of GI
195 symptoms on COVID-19 outcomes. Herein, we adjusted for age, body mass index (BMI), gender,
196 race, diabetes, HTN, chronic lung disease and heart disease in a multivariate model to determine
197 the impact of any GI symptoms and each of the individual GI symptoms (nausea, vomiting or
198 diarrhea) on disease outcomes. In the multivariable models, any GI symptoms, diarrhea, nausea,
199 and vomiting, were inversely associated with disease severity and mortality, while age and BMI
200 were positively associated with these outcomes. African-American race was inversely associated
201 with disease severity but not mortality (**Fig. 1c, Supplementary Fig. 2b, Supplementary Table**
202 **2).** Patients who presented with GI symptoms had 50% reduced odds of having severe disease
203 (odds ratio of 0.56) and death from COVID-19 (odds ratio 0.54), compared to the patients who
204 presented without GI symptoms (**Fig. 1d, Supplementary Table 2**).
205
206 **An external validation cohort further confirms decreased mortality in COVID-19 patients**
207 **with GI symptoms**
208 Next, we sought an external validation cohort, distinct from the MSH discovery cohort, and studied
209 well-characterized patients (n=287) from Milan, Italy, to determine the impact of GI symptoms on
210 COVID-19 associated outcomes. In this cohort, GI symptoms on admission were characterized
211 as presence (n=80, 27.9%) or absence of diarrhea on admission (**Table 5**). Consistent with the
212 discovery cohort, patients with diarrhea on admission were significantly younger (60.6 ± 13.9 vs
213 65.5 ± 13.3 for patients without diarrhea, $p = 0.0056$) and had significantly lower mortality (10.0%
214 in patients with diarrhea vs 23.7% in patients without diarrhea, $p=0.008$). Additionally, patients
215 with diarrhea had lower composite outcome of mortality or ICU admission compared to those
216 without diarrhea (20% vs 40%, $p=0.0014$) (**Table 5**). Distinct from the discovery cohort, the
217 proportion of male patients was lower in those patients with diarrhea (57.5%) compared to those
218 without diarrhea on admission (72%) ($p=0.0238$) (**Table 5**). Next, the association between
219 diarrhea and mortality was evaluated by multivariate logistic regression adjusting for age, gender,
220 BMI, diabetes, chronic heart and lung disease and other confounders. Even after adjusting for
221 these covariates, the presence of diarrhea on admission was found to be significantly inversely

222 associated with mortality with a median odds ratio of 0.33 over 1000 bootstrap iterations (**Fig.**
223 **1e**).

224 **Presence of GI symptoms can be used to predict reduced disease severity and mortality**
225 **in patients with COVID-19 in a second validation cohort**

226 After observing significantly reduced mortality in COVID-19 patients with GI symptoms in our
227 discovery and external validation cohort, we developed a predictive model based on the discovery
228 cohort and applied it to a distinct internal validation cohort comprising of 242 well-characterized
229 patients with COVID-19, admitted between April 16, 2020 and April 30, 2020 to MSH. The
230 inclusion of 'any GI symptoms' to a model consisting of age and BMI at baseline, improved the
231 ability to predict severity and mortality with a median area under the curve (AUC) of 0.59 (age +
232 BMI) vs. 0.64 (age + BMI + any GI symptoms) for disease severity and 0.70 (age + BMI) vs. 0.73
233 (age + BMI + any GI symptoms) for mortality (**Fig. 1f, Supplementary Table 3**). In addition, the
234 effect of GI symptoms, age and BMI on the AUC was evaluated by excluding each variable one
235 at a time from the model and calculating the consequent reduction in AUC. The exclusion of GI
236 symptoms resulted in a significant reduction in AUC with a median value of 0.054 for disease
237 severity and 0.03 for mortality. Notably, the effect of GI symptoms on the AUC was more dramatic
238 than that of age (AUC reduction of 0.054 versus 0.025) for disease severity (**Fig. 1f,**
239 **Supplementary Table 3**).

240

241 **COVID-19 patients with GI symptoms have reduced levels of circulating cytokines**
242 **associated with inflammation and tissue damage.**

243 To gain mechanistic insights into significantly reduced COVID-19 severity and mortality across
244 these three large cohorts, we began by analyzing systemic biomarkers, comparing patients with
245 and without GI symptoms admitted to MSH (discovery and internal validation cohorts). Initially,
246 we examined, a set of 4 cytokines, IL-6, IL-8, TNF-α, and IL-1β, measured on admission in all the
247 patients as part of routine clinical care. IL-6, and IL-8 levels, known to be associated with poor
248 survival[35] were found to be significantly reduced in circulation of patients with GI symptoms (FDR
249 10%) (**Supplementary Fig. 3, Supplementary Table 4).**

250 Next, to facilitate high dimensional analyses of potential immunological differences
251 between patients with and without GI symptoms, we performed a validated, multiplexed proteomic
252 assay (O-link), simultaneously quantifying 92 protein analytes in 238 patients (from among the
253 discovery and internal validation cohorts; GI symptoms (n=104), no GI symptoms (n=134)) where
254 serum samples were available for analyses. Unsupervised consensus clustering of these 92
255 analytes revealed six groups of analytes with similar expression patterns across all COVID-19

256 patients (**Fig. 2a, Supplementary Table 5**). Notably, analytes in clusters 5 and 6 displayed less
257 correlation in patients with GI symptoms compared to those without GI symptoms (**Fig. 2a**,
258 **Supplementary Fig. 4**). Next, we interrogated biological pathways over-represented in each
259 cluster of soluble analytes. We found that the “KEGG Jak/Stat Signaling Pathway” was
260 significantly enriched in Cluster 5; while the "Hallmark Inflammatory Response" pathway was
261 significantly enriched in Cluster 4 (Fisher’s exact test 10% FDR). These pathways were
262 downregulated in patients displaying diarrhea symptoms based on pathway level signatures
263 ($p<0.05$ from t-test) (**Fig. 2b**); suggesting a reduced inflammatory response in patients affected
264 by GI symptoms. In addition, we found that clusters 1, 2, 3, 5 and 6 were significantly
265 downregulated in patients with GI symptoms compared to those without (FDR 15%) (**Fig. 2c**).
266 This downregulation seemed to be driven mostly by diarrhea since the same clusters 1, 2, 3, 5
267 and 6 were significantly downregulated with FDR correction at 10% in patients who presented
268 with diarrhea compared to those without symptoms. The lack of signal registered for nausea and
269 vomiting might be due to reduced statistical power given by the smaller number of samples
270 displaying vomiting (n=29) or nausea (n=54) symptoms.
271 When looking at each of the 92 analytes individually, key inflammatory cytokines and
272 chemokines were significantly downregulated (IL-8, TGF-α, IL-17C, IL-15RA, IL-10RB, MMP10,
273 TNFRSF9, OPG, IL-6, LIF, GDNF, IL-17A, ARTN and CCL28). On the other hand, TNF-Related
274 Apoptosis Inducing Ligand (TRAIL), a cytokine with immune regulatory properties[42,43] and IL-7, a
275 cytokine associated with T cell development[44] were significantly upregulated in patients with GI
276 symptoms compared to those without (t-test FDR 10%) (**Fig. 2d,e, Supplementary Table 6**).
277 When looking at each individual GI symptom, diarrhea had the most significantly differential
278 analytes. As a caveat, this difference between diarrhea, nausea and vomiting might be due to
279 reduced statistical power given that fewer patients presented with nausea and vomiting than those
280 who presented with diarrhea. Consistent with GI symptoms as a group, IL-7 was significantly
281 increased, in addition, MCP-2 was significantly increased in patients presenting with diarrhea.
282 We also quantified total anti-spike protein IgA, IgG and IgM antibodies and compared
283 patients with and without GI symptoms and patients with and without diarrhea. There were no
284 significant differences between the groups (**Supplementary Fig. 5**)
285 Thus, overall, GI symptoms are associated with significantly reduced levels of key
286 inflammatory cytokines like IL-6, IL-8, IL-17 and CCL28 that are known to be associated with poor
287 COVID-19 outcomes.
288
289 **The GI tract was endoscopically uninflamed in all patients**

290 Next, we sought to obtain GI tissue-level mechanistic insights regarding disease pathogenesis.
291 To this end, we enrolled 18 cases with COVID-19 and 10 SARS-CoV-2 uninfected controls who
292 underwent upper GI endoscopy (SARS-CoV-2 infected n=16, uninfected n=8), colonoscopy
293 (SARS-CoV-2 infected n=1, uninfected n=1) or both upper endoscopy and colonoscopy (SARS-
294 CoV-2 infected n=1, uninfected n=1) (**Table 6, Supplementary Table 7**). Patient 10 was initially
295 suspected to have COVID-19 but was excluded after multiple negative SARS-CoV-2
296 nasopharyngeal (NP) PCR tests and negative COVID-19 antibody tests. The remaining 17 cases
297 were classified as asymptomatic / mild / moderate (n=10) or severe (n=7) disease according to
298 the criteria detailed in **Supplementary Table 1**. While we endeavored to examine patients as
299 early in disease course as was possible, given the aerosolizing nature of endoscopic procedures
300 (potentially exposing endoscopic staff to SARS-CoV-2), as well as challenges inherent in
301 endoscopic biopsies of acutely ill COVID-19 patients, a majority of patients were examined in the
302 early convalescent phase of COVID-19 disease. Specifically, GI biopsies were performed after
303 27.5 ± 13.8 days from the onset of COVID-19 symptoms (or first SARS-CoV-2 PCR if
304 asymptomatic) and 17.3 ± 17.5 days from the last positive NP swab (if patient had a positive NP
305 swab after the procedure, it was considered to be 0 days from last PCR positive) (**Fig. 3a**).
306 COVID-19 symptoms on presentation and treatment regimens were diverse as detailed in
307 **Supplementary Table 8**. Sample allocation for different assays is detailed in **Supplementary**
308 **Fig. 9**.
309 The GI mucosa was endoscopically uninflamed in all subjects regardless of the severity
310 of illness, with no evidence of loss of vascularity, edema, friability, erosions or ulcerations (**Fig.**
311 **3b**), except for one post-intestinal transplant case where inflammation was attributed to transplant
312 rejection. Histopathological examination revealed a mild increase in intraepithelial lymphocytes
313 (IELs) in 8 cases and a scant neutrophilic infiltrate in 7 cases (**Fig. 3c**, **Supplementary Fig. 6**,
314 **Supplementary Table 9**). Notably, the biopsies were reported as histologically normal in 3 cases
315 (**Fig. 3d, Supplementary Table 9**). Histopathological details of pre-pandemic (non-COVID-19)
316 controls are provided in **Supplementary Table 10**.
317
318 **Small bowel enterocytes have robust expression of Angiotensin converting enzyme-2**
319 **(ACE2) and harbor SARS-CoV-2 antigens**
320 Early events in the pathogenesis of SARS-CoV-2 infection include attachment of the receptor
321 binding domain of the viral spike (S) protein to epithelial ACE2[14-17]. Using immunofluorescence
322 (IF) microscopy, we observed robust and extensive expression of ACE2 on the small intestinal
323 brush border in both COVID-19 cases and controls (**Fig. 4a-h**). Additionally, we detected SARS-

CoV-2 nucleocapsid protein in small intestinal enterocytes of COVID-19 patients (**Fig. 4i,n, Supplementary Fig. 7**), but not controls (**Fig. 4m,r, Supplementary Fig. 8**), indicative of virus infection in these cells. Remarkably, when present, the distribution of viral antigens was patchy in the upper small intestines (duodenum; **Fig. 4i-l**), but diffuse in the lower small intestines (ileum; **Fig. 4n-q**). Positive staining was exclusively seen in the epithelium irrespective of intestinal location. Overall, of the 11 COVID-19 patients where IF staining was performed, 10 showed viral antigen on IF microscopy in at least one intestinal segment (duodenum or ileum) (**Supplementary Table 9**). Interestingly, the presence of viral antigens on IF did not correlate with the presence of histologic abnormalities. As negative controls, 5 duodenal biopsies and 6 ileal biopsies from 10 patients collected prior to the pandemic (**Supplementary Table 10**), showed no evidence of viral antigens on immunostaining (**Fig. 4m,r, Supplementary Fig. 8**).

Ultrastructural analyses of GI tissues reveal viral particles in small intestinal enterocytes

Transmission electron microscopy of intestinal biopsy tissues revealed the presence of 70-110 nm viral particles in the enterocytes of the duodenum and ileum (**Fig. 4s-u**). Pleomorphic, spherical structures, morphologically consistent with viral particles were observed in conjunction with small vesicles within enterocytes along the basolateral surface of the enterocytes (**Fig. 4s**) and blebbing off of the enterocyte apex (**Fig. 4u**). Particles with distinct, stalk-like projections (corona) were seen within the enterocyte cytoplasm (**Fig. 4t**). Overall, of the 13 patient samples processed for electron microscopy studies, 6 showed viral-like particles on ultrastructural analyses (**Supplementary Table 9**).

Infectious virions could not be isolated from the GI tissues of COVID-19 patients

Several attempts were made to assess for the presence of potentially infectious virions in the intestines of COVID-19 patients. Supernatants of homogenized intestinal tissues were inoculated on confluent Vero E6 cells and incubated at 37℃ for 7 days. Brightfield microscopy showed no apparent cytopathic effects (CPE). In addition, cell culture supernatants did not reveal the presence of viral RNA by quantitative RT-PCR (qRT-PCR) and plaque assays. Experiments showed no plaque formation in Vero E6 cells after staining with 2% crystal violet solution.

RT-qPCR was performed in whole biopsy tissue after RNA isolation in both COVID-19+ patients and controls. Results showed that Ct values of COVID-19+ patients were ≥34, while RNA sequencing (RNA-Seq) data detected SARS-CoV-2 reads only in the one ileal sample tested but in none of the 12 duodenal biopsies. Altogether these data suggest that SARS-CoV-2 was present at low copy numbers in the GI tract of these early-convalescent COVID-19 cases.

358

359 **GI lamina propria pro-inflammatory dendritic cells are depleted in COVID-19 patients**

360 Next, we performed mass cytometry (CyTOF) based immunophenotypic analyses on the GI
361 tissues of 13 and peripheral blood of 10 COVID-19 cases and 10 controls (**Table 6,**
362 **Supplementary Table 7, Supplementary Fig. 9**). GI tissues were divided into lamina propria
363 (LP) and epithelial compartment (EC) fractions and analyzed separately. Immune populations
364 were clustered on the basis of cell-specific markers for both the LP and EC (**Fig. 5a,c,g**). While
365 the overall distribution of canonical immune cell subsets in the GI LP were comparable between
366 COVID-19 and control patients (**Fig. 5a,b**), few immune populations showed differences as
367 detailed below. Additionally, no clear differences in the LP could be discerned between patients
368 with asymptomatic/mild/moderate disease and those with severe disease (**Fig. 5b,**
369 **Supplementary Table 12a**).

370 In the LP, among myeloid cells, $CD206^+CD1c^+$ "inflammatory" cDC2 (conventional DCs)[45]
371 were reduced in COVID-19 cases compared to controls (0.4-fold decrease, p=0.01). Additionally,
372 plasmacytoid DCs (pDCs) were reduced in COVID-19 cases (0.5 fold decrease, p=0.07) (**Fig.**
373 **5d,e**), analogous to changes described in the peripheral blood of COVID-19 patients[36]. Among
374 other LP populations, effector ($PD\text{-}1^+CD38^+$) $CD4^+$ and $CD8^+$ T cells were significantly increased
375 in COVID-19 cases compared to the controls (**Fig. 5f**), while $CD8^+CD103^+$ T cells (tissue resident
376 memory subset) trended higher in COVID-19 cases compared to controls (1.7-fold increase,
377 p=0.06) (**Supplementary Fig. 10a**). Neutrophils (3-fold), eosinophils (1.9-fold), $CD4^-CD8^-$T cells
378 (3.5-fold) and $CD4^+CD103^+$ T cells (1.8-fold) were increased in COVID-19 cases, but these
379 differences were not statistically significant possibly due to the sample size. We also observed a
380 trend of non-significantly decreased regulatory $CD4^+$ T (T_{REG}) cells (0.6-fold decrease) and
381 increased IgM^+ plasma cells (2.3-fold increase) in the LP of infected cases vs controls
382 (**Supplementary Fig. 10a**). The distribution of naïve and memory $CD4^+$ and $CD8^+$ T cells was
383 altered in COVID-19 patients, with a reduction of naïve $CD4^+$ T cells and EMRA (effector memory
384 re-expressing RA) $CD8^+$ T cells in LP of COVID-19 patients (**Supplementary Fig. 10b**), but this
385 difference did not reach statistical significance.

386 Similar to the LP, the EC showed a reduction of $CD206^+$ cDC2 in COVID-19 cases
387 compared to controls (0.4-fold decrease, p=0.05), while the $CD4^-CD8^-$ subset of IELs was
388 significantly increased (1.6-fold-increase, p=0.03) (**Fig. 5h**). $CD8^+$ T cells, the dominant IEL
389 population, showed an increase (2.6-fold) in COVID-19 cases compared to controls but the
390 difference did not reach statistical significance (p=0.4) (**Supplementary Table 12a**), likely owing
391 to inter-patient variability, also observed by light microscopy. A subset of $CD8^+$ IELs, $CD8^+CD69^+$

392 T cells, showed a non-significant increase in COVID-19 cases vs controls (3.9-fold, p=0.2), while
393 plasma cells were comparable between the cases and controls (**Supplementary Fig. 11 a,b,c)**.
394 In the peripheral blood, cell type assignments were carried out using specific cell surface
395 markers (**Supplementary Fig. 12a**). We observed that effector (PD-1$^+$CD38$^+$) T cells (for both
396 CD4$^+$ and CD8$^+$ T lymphocytes) were significantly increased in PBMCs of SARS-CoV-2 infected
397 individuals (**Fig. 5i**). CD14$^-$CD16$^+$ inflammatory monocytes trended lower in COVID-19 cases
398 compared to controls (0.4-fold decrease, p=0.09). In contrast, CD14$^+$CD16$^-$ "classical" monocytes
399 were comparable in COVID-19 cases and controls (p=0.3) (**Supplementary Fig. 12b**).
400 Additionally, a non-significant increase in IgG$^+$ plasma cells (7.2-fold, p=0.13) and a non-
401 significant decrease in T_{REG} (0.8-fold, p=0.2) were observed in COVID-19 cases (**Supplementary**
402 **Fig. 12c,d, Supplementary Table 12b**). Finally, a significant increase in activated (CD29$^+$CD38$^+$)
403 CD4+ T cells was noted in the peripheral blood of COVID-19 cases compared to controls
404 (**Supplementary Fig. 13a)** and a non-significant increase of these activated T cells in the LP of
405 COVID-19 patients (**Supplementary Fig. 13b**)**.** Details of all immune population changes in the
406 GI LP, GI EC and in circulation are provided in **Supplementary Table 12a and 12b**.
407 Altogether, similar to published data from the peripheral blood of COVID-19 patients[36],
408 intestinal tissues from COVID-19 cases showed reduced pro-inflammatory DCs and pDCs but
409 increased effector T cells compared to controls.
410
411 **GI LP pro-inflammatory pathways are downregulated in COVID-19 patients**
412 To further probe the molecular response of the GI tract following SARS-CoV-2 infection, we
413 performed RNA-Seq on EC and LP cellular fractions separately in 13 COVID-19 patients and 8
414 controls. Samples derived from the EC and LP clustered separately on the basis of their top
415 transcriptional signatures, demonstrating distinctness of the two compartments within the GI tract
416 (**Supplementary Fig. 14, Supplementary Data**). Accordingly, comparisons between COVID-19
417 cases and controls were performed separately for each tissue, and 1063 differentially expressed
418 genes (DEG) were identified out of total 11419 genes detected (**Fig. 6a, Supplementary Data**).
419 The majority of DEGs were detected in the LP (1061, false discovery rate [FDR] $\leq$ 0.05), compared
420 to 12 DEGs in the EC that largely overlapped with the LP (**Fig. 6a**). Both LP and EC showed
421 upregulation of genes involved in immunomodulation, including the anti-microbial peptide *LCN2*,
422 and the metallothioneins *MT1E*, *MT1F*, *MT1H*, *MT1M*, *MT1X*, *MT2A* and *TMEM107.* In addition,
423 heat shock proteins, *HSPA1A* and *HASPA1B,* were downregulated in both tissues. Pathway
424 enrichment analysis of DEGs ranked by significance revealed several KEGG pathways that were
425 depleted in COVID-19 patients compared to controls (**Fig. 6b)**. Downregulation of pathways linked

426 to T_H17 cell differentiation and inflammatory bowel diseases (IBD) was characterized by the
427 depletion of *RORA, IL4R, IFNG, IL18R1, IL1B, STAT4* and *HLA-DRA*. Pathways linked to antigen
428 processing, T_H1 and T_H2 cell differentiation, and MAPK signaling were significantly downregulated
429 in the LP from COVID-19 patients. In contrast, genes associated with metabolic functions,
430 including amino acid metabolism (*NOS2, SMS, ALDH2, GOT2*), mineral absorption (*MT1G,*
431 *MT2A, MT1E*), as well as mucin biosynthesis (*GALNT7, GALNT3, GALNT8*) were significantly
432 upregulated in COVID-19 patients compared to controls (**Fig. 6b**).

433 We considered the possibility that the observed expression changes could imply
434 alterations in relative cell type proportions (in addition to transcriptional alterations within cells).
435 Therefore, we interrogated GI data derived from single-cell RNA-seq[46] for enrichment of cell type-
436 specific gene expression signatures. Consistent with CyTOF data (**Fig. 5** and **Supplementary**
437 **Table 12a and 12b**), genes associated with DCs and eosinophils were reduced in COVID-19
438 patients compared to controls (**Fig. 6c**). Additionally, signatures related to the size of endothelial
439 cell and mast cell pools were reduced, while genes linked to goblet cells, proliferating epithelial
440 cells, enteroendocrine cells and epithelial stem cells were increased, possibly reflecting the
441 sequelae of intestinal epithelial infection by SARS-CoV-2 and subsequent recovery (**Fig. 6c**).

442 Given the unexpected reduction in DC numbers in the GI tissues, we probed myeloid gene
443 signatures further, and found significant downregulation of genes associated with pDC *(DAPK1,*
444 *IRF7, ICAM1* and *GM2A*), activated DCs (*TNFAIP2, CD86, CD83*), cDC1 (*RELB, IRF8* and *HLA-*
445 *DRA*) and cDC2 (*CLEC7A* and *CLEC10A*). Of note, we also found that LP genes associated with
446 inflammatory DCs (monocyte-derived DCs, MoDCs) (*TGFBI, TGFB1, STAB1, SDCBP,*
447 *RNASET2, MSR1, MRC1, MERTK, DNASE1L3, CD163L1, C5AR1, SPI1, CSF1R, AOAH, ABCA*)
448 were significantly reduced (**Fig. 6d**), which was consistent with the reduced number of
449 inflammatory DCs observed by CyTOF.

450 Finally, we looked at the average EC and LP expression of recently reported gene
451 signatures linked to the antiviral response against SARS-CoV-2 from post-mortem lung tissue
452 samples[30], and human intestinal organoids[29]. Although we did not observe a substantial acute
453 SARS-CoV-2 response, there was significant upregulation of *LCN2* in both EC and LP, and *OAS*
454 and *GBP3* in the LP only. Notably, we did observe a trend towards induction of antiviral response
455 genes in the EC, where expression of canonical antiviral genes such as *IFI44L, IFIT1, IFITM3,*
456 *IFI44, IFI6* and *OAS3* was increased (**Fig. 6e**).

457 Next, using gene set enrichment analysis (GSEA), we rank ordered the EC DEGs
458 according to effect size (logFC * -logPvalue) and tested for enrichment in the reported SARS-
459 CoV-2 infected gene signatures[29] (**Supplementary Fig. 15a**). The genes upregulated in EC

460 showed a significant enrichment in genes upregulated in the SARS-CoV-2 infected intestinal
461 organoid gene datasets. We then carried out Hallmark pathway enrichment analyses on this
462 ranked EC gene list and found that the top two processes associated with genes upregulated in
463 EC were interferon alpha response (normalized enrichment score (NES) 1.91, FDR<0.005) and
464 interferon gamma response (NES=1.8, FDR=0.005) (**Supplementary Fig. 15b**). This enrichment
465 is indicative of the host antiviral response against SARS-CoV-2 in human intestines of COVID-19
466 patients.

467 We then evaluated cytokines and chemokines in intestinal samples projecting our RNA-
468 seq dataset with published data from the human bronchial epithelial cells infected with SARS-
469 CoV-2[30]. Remarkably, we found that the many of the inflammatory cytokines and chemokines
470 such as IL-1β, IFNγ, CCL24 and CXCL8 were downregulated in COVID-19 patients (**Fig. 6e**). The
471 only chemokine showing significant increase was CCL15 which is reported to have structural
472 properties of antimicrobial peptides and has a role in maintaining intestinal homeostasis[47] (**Fig.
473 6e**). Significantly, we also noted that the key inflammatory genes including *IFNG, IL1B, CXCR4,
474 TNFSF14, CXCL2, CSF-1, CXCL8, IL18R1, NRP1 and IL18BP* were downregulated in intestinal
475 LP of COVID-19 cases compared to the uninfected controls (**Fig. 6f**).

476 Together, these data reveal a dynamic remodeling of GI tissues by SARS-CoV-2, notable
477 in the LP for a significant downregulation of pathways associated with inflammation and antigen
478 presentation, yet activation of viral response signaling genes in the EC.

479

480 **Discussion**

481 At the outset, given the robust expression of ACE2 on the small intestinal epithelium[48], at
482 levels that are arguably among the highest in the body[49], we hypothesized that the GI tract would
483 be susceptible to SARS-CoV-2 infection. In testing our hypothesis, herein, we report on the first
484 human study to demonstrate infection of intestinal enterocytes *in vivo*, define the cellular and
485 transcriptomic responses of GI tissue in COVID-19 patients and associate them with clinical
486 outcomes in multiple, large cohorts of COVID-19 patients. An unexpected, but significant
487 reduction in disease severity and mortality in patients with GI symptoms identifies a new aspect
488 of disease pathogenesis and provides evidence of an 'organ-specific' program of host response
489 to SARS-CoV-2, which in this case is associated with a survival advantage.

490 GI manifestations, reported in nearly half of patients within our discovery cohort were
491 notably higher than some of the early reports[3,7] but similar to more recent studies[8], likely
492 attributable to greater clinical awareness of GI symptoms and therefore more documentation of
493 such symptoms. A recently published study of 278 patients from a Columbia University Hospital

494 in New York City reported that among COVID-19 patients with GI symptoms (diarrhea, nausea
495 and vomiting), there was a non-significant trend towards lower rates of intensive care unit (ICU)
496 admission and a significantly lower rate of death during short-term follow-up[50]. Similar
497 observations arise from the study of 'Multisystem Inflammatory Syndrome Children' (MIS-C).
498 Some of these children have diarrhea as a predominant symptom[51,52], systemic evidence of GI
499 involvement[9,53,54], and a unique responsiveness to anti-inflammatory treatments, including IL-6,
500 intravenous immunoglobulin (IVIG) and anti-IL1[55-58], which lead to the resolution of inflammatory
501 pathology in these children. Intestinal involvement in COVID-19 resulting in mortality benefit
502 stands in contrast to the involvement of all other organs including the pulmonary[59,60], renal[61,62]
503 and vascular[63] compartments.

504 The fact that GI symptoms remain significantly associated with better COVID-19 outcomes
505 after adjusting for multiple covariates, known to be associated with reduced survival, in 3
506 independent cohorts totaling 1163 patients, across two different countries enhances the
507 robustness and validity of our findings. Furthermore, our model to predict COVID-19 severity and
508 mortality was enhanced by the inclusion of GI symptoms suggesting that intestinal parameters
509 should be considered in initial assessments and severity stratification of COVID-19 patients.

510 Several, non-mutually exclusive hypotheses may explain the lower mortality in COVID-19
511 patients with GI symptoms. Possibilities include "diversion" of the virus away from the lung, an
512 organ where infection proves lethal in a subset of patients. Another possibility includes virus
513 intrinsic factors, associated with differences in tissue-tropism and perhaps virulence. Yet another
514 intriguing possibility is that GI infection stimulates an anti-inflammatory, 'tolerogenic' immune
515 response locally as well as systemically. Detailed examination of soluble, cellular and
516 transcriptomic factors associated with GI infection provided some support for this argument.

517 For example, independent of disease severity and unlike inflammatory changes seen in
518 the pulmonary mucosa[64], inflammatory infiltrates were scarce in the LP of COVID-19 patients. A
519 patchy and mild increase in IELs was observed within the EC. Additionally, we observed a rather
520 significant lack of cDC2, 'inflammatory' DCs, pDCs in the intestinal LP. These findings mirror
521 observations from the SARS epidemic of 2003[19] as well as current autopsy data demonstrating a
522 lack of intestinal inflammation despite the presence of viral antigens in both these tissues[65]. We
523 propose that, in spite of their infectability, the intestines mount a limited and short-lasting
524 inflammatory response to SARS-CoV-2.

525 On examination of circulating proteins, including analyses of cytokines and chemokines
526 known to be associated with COVID-19 severity[30,31,35], we found that multiple
527 cytokines/chemokines were downregulated in patients with GI symptoms compared to patients

528 without. These included the proinflammatory cytokines IL-6 and IL-8, which are now considered
529 a hallmark of increased severity and mortality in COVID-19 as well as a number of other
530 cytokines/chemokines involved in tissue inflammation. The lower IL-17 expression we observed
531 systemically is in line with the reduced T_H17 RNA seq expression signatures we found in biopsy
532 samples from COVID-19 patients. IL-17 is secreted by T_H17 and innate cells and is crucial for the
533 recruitment of neutrophils promoting inflammation in a variety of tissues, including the intestinal
534 mucosa[66,67]. Additionally, IL-17 has been shown to have pathogenic effects both in SARS-CoV-
535 2[68] as well as during SARS-CoV[69] and MERS[70] infections. Interesting, IL-17C (specifically found
536 to be decreased in patients with GI symptoms in our study) is produced primarily by epithelial
537 cells rather than hematopoietic cells[71]. Our finding of COVID-19 patients with GI symptoms having
538 reduced CCL28, a cytokine expressed by mucosal epithelial cells and involved in eosinophil
539 chemotaxis[72], is consistent with prior work showing increased eosinophils to be associated with
540 severe COVID-19 disease[31] and our RNA-seq data showing decreased eosinophil associated
541 genes. IL-15 promotes neutrophilic cytoplasmic re-arrangements and phagocytosis[73], DCs
542 differentiation[74], and T cell stimulation[75]. The reduced systemic expression of the IL-15 receptor
543 is in line with our intestinal findings showing lower frequencies of DCs in COVID-19 patients. IL-
544 10 is generally considered an immune modulatory and anti-inflammatory cytokine, however an
545 excess of IL-10 can inhibit the function of immune cells such as NK and CD8+ T cells, possibly
546 delaying clearance of viruses[76]. Our results of increased systemic expression of IL-10 receptor in
547 patients presenting without GI symptoms is in line with previous studies showing IL-10 to be
548 elevated in COVID-19 patients, associated with disease severity and inversely correlated with
549 $CD8^+$ T cells[77,78].

550 In contrast, the only two cytokines found to be upregulated in patients presenting with GI
551 symptoms were IL-7 and TRAIL, both with important immunoregulatory functions. IL-7, produced
552 by stromal cells and intestinal epithelial cells, has been considered as a therapeutic agent in
553 COVID-19 related to its effects on T cell differentiation and survival[79]. Similarly, TRAIL is
554 associated with immunosuppressive, immunoregulatory and anti-inflammatory functions[42,43] as
555 well as some evidence of viral infection control in the intestinal tract[80].

556 Transcriptome analyses further demonstrated the downregulation of a number of
557 important pro-inflammatory gene products, including *IFNG*, *IL1B*, *IKBKB* and *STAT3B, which*
558 contribute to T_H17 cell differentiation and IBD pathogenesis. Calprotectin, a heterodimer
559 encompassing calgranulin A and calgranulin B, which are encoded by *S100A8* and *S100A9*,
560 respectively, was recently identified as a biomarker of severe COVID-19 disease and suggested
561 to represent a trigger of cytokine release syndrome[81]. We observed no induction of *S100A8* or

562 *S100A9* in intestinal tissues, even in patients with severe COVID-19, suggesting that the vast
563 intestinal surface did not contribute to the production of calprotectin in COVID-19 patients. Pro-
564 inflammatory cytokines and chemokines that are elevated in the lungs of COVID-19 patients[64,82]
565 were surprisingly downregulated (*IL1B, CXCL8, CXCL2, CXCR6*) or unchanged (*CCL3*, *CXCL10,*
566 *CCR1, CXCR3*) in the intestines, compared to non-COVID controls. Other relevant gene products
567 associated with severe COVID-19[64,83,84] were either significantly lower in the intestinal LP
568 (*CXCL8*, *IL1B, IFNG, HIF1A, HLA-DQA1*) or trended lower (*CCL2*, *CCL4*, *CCL4L2*, *CTSB*, *IL23A*)
569 or were comparable to non-COVID controls (*HMGB1*, *CCL3*, *CCL8*, *HMOX1*). Tissue-residence
570 markers such as *ITGA1*, *CXCR6*, *JAML*, which are reported to be increased in the pulmonary
571 mucosa of severe COVID-19 patients[64], were significantly downregulated in the GI tract. Finally,
572 aside from detecting decreased expression of pro-inflammatory gene products, we found
573 increased expression of anti-inflammatory gene products, including transcripts involved in the
574 biogenesis of the gut-specific MUC2 mucin, a mucus-forming glycoprotein released by goblet
575 cells that contributes to gut tolerance[85].
576 Thus, by dissecting circulating proteomic and GI tissue transcriptomic response, we noted
577 a cytokine milieu characterized by either a suppression of or a failure of induction of an
578 inflammatory response to the virus. Additionally, we observed a lack of production of secondary
579 mediators including calprotectin, which would feed into the inflammatory cascade and culminate
580 in the "cytokine storm" typical of severe COVID-19. Our detailed cellular analyses confirm a lack
581 of inflammatory monocytes and macrophages and a depletion of inflammatory DCs in the GI tract.
582 This failure of induction of inflammatory pathways, regardless of the clinical severity of disease,
583 stands in stark contrast to the massive immunopathology, noted systemically, and within the
584 pulmonary mucosa of severe COVID-19 patients[60] as well as patients with active IBD[86,87].
585 The mechanisms underpinning the lack of inflammation in the COVID-19-infected intestine
586 are unclear, but could be linked to the notorious tolerogenic bias of both effector and regulatory
587 cells from both innate and adaptive branches of the mucosal immune system[88]. In addition, the
588 SARS-CoV-2 virus could specifically inhibit immune activating and/or stimulate immune
589 suppressive pathways in the intestinal mucosa directly or indirectly through ACE2 or other
590 receptors. We also recognize that our analyses of the GI tract were not performed during the most
591 acute phase of the illness in some patients. However, even in the patients that were sampled
592 within the first 15 days of the onset of symptoms or positive nasal swab (patients 1, 6 and 18),
593 the "pro-inflammatory changes" were not observed in the intestines. A separate study by our
594 group that analyzed stool samples from patients going through the acute phase of COVID-19,
595 found little evidence of an active gut inflammatory response. In particular, such stool samples

596 strikingly lacked any significant increase of IL-1β, IL-6, TNF-α and IL-10, despite the detection of
597 viral genomes (MEDRXIV/2020/183947).
598 In summary, we have observed an unexpected but significant reduction in COVID-19
599 severity and mortality when patients demonstrate GI symptoms like diarrhea, nausea or vomiting.
600 These data suggest a previously unappreciated tissue-specific response to SARS-CoV-2 and
601 provide the rationale for more studies aimed at determining the mechanisms underpinning the
602 attenuation of SARS-CoV-2 pathogenicity by the intestinal environment. Such efforts may lead to
603 the development of novel treatments against COVID-19 and potentially other similar deadly
604 infections in the future.
605
606 **Methods**
607 **Clinical cohorts**
608 *1. Discovery cohort*
609 Patients admitted to Mount Sinai Hospital (MSH) between April 1, 2020 and April 15, 2020 were
610 recruited into the Discovery Cohort if they were SARS-CoV-2 PCR positive, more than 18 years
611 of age and if the "ELLA panel of cytokines" (IL-6, IL-8, IL-1β and TNF-α) was performed as part
612 of clinical care. Clinical details from eligible patients were extracted from Mount Sinai Data
613 Warehouse (MSDW) under an IRB approved protocol (IRB-20-03297A North American registry
614 of the digestive manifestations of COVID-19)
615 A total of 634 subjects were included in the discovery cohort (**Supplementary Figure 1**).
616 In addition to demographic information (including race and ethnicity and primary language),
617 clinical characteristics, laboratory data and outcomes data was extracted from the medical charts.
618 Co-variates that were studied included: history of smoking, BMI (obesity defined as BMI >30) and
619 comorbid conditions including, hypertension, diabetes, chronic lung disease (including asthma
620 and COPD), heart disease (including coronary artery disease, atrial fibrillation and heart failure),
621 chronic kidney disease, cancer, HIV, and inflammatory bowel disease (IBD).
622 COVID severity was defined based on internal scoring system developed by the
623 Department of Infectious Diseases at Mount Sinai Hospital with the following definitions: Mild -
624 SpO2>94% on room air AND no pneumonia on imaging, Moderate - SpO2<94% on room air OR
625 pneumonia on imaging, Severe - high flow nasal cannula (HFNC), non-rebreather mask (NRBM),
626 Bilevel Positive Airway Pressure (non-invasive positive airway ventilation), or Mechanical
627 ventilation AND no pressor medications AND creatinine clearance > 30 AND ALT < 5x upper limit
628 of normal, Severe with evidence of end organ damage (EOD) - high flow nasal canula (HFNC),
629 non-rebreather mask (NRBM), Bilevel Positive Airway Pressure (non-invasive positive airway

630 ventilation), or Mechanical ventilation AND pressor medications OR creatinine clearance <30 OR
631 new renal replacement therapy OR ALT > 5x upper limit of normal.
632 GI symptoms were defined as more than one episode of either diarrhea, nausea, and/or
633 vomiting at the time of admission. If only one episode of either diarrhea, nausea, and/or vomiting
634 was specifically documented, patients were not considered to have GI symptoms. Additionally,
635 we did not consider GI symptoms that developed during the course of hospitalization, as they
636 could reflect nosocomial or treatment-related effects.
637 Disease severity (as described above) and mortality were considered as outcomes
638 variables. Mortality was calculated as patient status (dead or alive) at 25 days post admission. If
639 no information was available after discharge, patients were censored at the time of hospital
640 discharge.

641 *2. External Validation Cohort*

642 To confirm the Discovery Cohort findings, we analyzed a cohort of patients admitted to a tertiary
643 care center in Milan, Italy between February 22, 2020 and March 30, 2020. A total of 287 patients
644 with a confirmed positive SARS-CoV-2 PCR and who did not die or were not transferred to the
645 ICU within 24 hours from admission were studied. Presence of vomiting and diarrhea (defined
646 as at least three loose bowel movement per day) on or prior to admission was recorded. Outcomes
647 were analyzed using ICU admission, death or the composite study end-point of ICU admission or
648 death within 20 days of hospitalization.

649 *3. Internal Validation Cohort*

650 To test a predictive model of COVID-19 severity and disease-related mortality, we developed a
651 distinct 'Internal Validation Cohort' of patients who were hospitalized at MSH between April 16,
652 2020 and April 30, 2020 and satisfied the same inclusion and exclusion criteria as in the discovery
653 cohort. Additionally, patients already included in the discovery cohort were excluded. From a total
654 of 408 patients, 242 met inclusion criteria and were thus included in the Internal Validation Cohort.
655 Demographic, clinical and outcomes related data was extracted from patients' medical records
656 as described for the Discovery Cohort.

657 *4. Intestinal Biopsy Cohort*

658 To gain mechanistic insights into GI tissue response in COVID-19 patients, intestinal biopsies and
659 peripheral blood from 18 COVID-19 and 10 control patients were obtained between April 17, 2020
660 and June 2, 2020. Subjects included hospitalized patients as well as those seen in the outpatient
661 GI practices. COVID-19 cases and controls were defined on the basis of SARS-CoV-2 swab tests.
662 The demographic characteristics of these patients and controls are provided in **Fig. 3a, Table 6,**

663 and **Supplementary Table 7**. Informed consent was obtained from all patients. The biopsy-
664 related studies were approved by the Mount Sinai Ethics Committee/IRB (IRB 16-0583, The
665 impact of viral infections and their treatment on gastrointestinal immune cells).
666
667 **SARS-CoV-2 testing**
668 The SARS-CoV-2 PCR was run in the Clinical Microbiology laboratory as part of routine care on
669 the Roche cobas platform. This platform performs selective amplification of 2 targets ORF-1
670 (Target 1) and the E-gene for pan-Sarbecovirus (Target 2) (detects SARS-CoV-2 as well as SARS
671 or MERS viruses, but not routine seasonal Coronavirus). A positive result indicated that either
672 both Target 1 and Target 2 were detected (majority of cases) or Target 1 alone was detected. A
673 presumptive positive result indicates a negative Target 1 result and a positive Target 2 result
674 which according to the manufacture can be a result of the following: “1) a sample at concentrations
675 near or below the limit of detection of the test, 2) a mutation in the Target 1 target region in the
676 oligo binding sites, or 3) infection with some other Sarbecovirus (e.g., SARS-CoV or some other
677 Sarbecovirus previously unknown to infect humans), or 4) other factors." Patients with a
678 presumptive positive SARS-CoV-2 PCR were included in the analysis if they were treated
679 clinically as having COVID-19.
680
681 **Computational analyses**
682 *Descriptive statistics*
683 Basic demographics and clinical characteristics of the cohort were defined by descriptive
684 statistics. For univariable analyses graph pad prism (version 8) was used to perform statistical
685 analyses and to produce figures. For age, an unpaired t-test was performed. For categorical
686 variables, the Fisher’s exact test or the Chi-square test was used as appropriate.

687 *Multivariate model based on discovery cohort*
688 For this analysis, we considered 570 patients with clinical descriptors including as age, gender,
689 race, BMI, comorbidities and GI symptoms. A multivariate logistic regression was utilized to model
690 severity and mortality as function of each of the GI symptoms and clinical variables including race,
691 age, gender, BMI, heart and lung diseases and hypertension. In particular, race was stratified as
692 White (Caucasian), Black (African-American), Hispanic and others; lung disease was set equal to
693 1 if the patient was either affected by COPD or asthma and zero otherwise; heart disease was
694 set equal to 1 if the patient was either affected by coronary artery disease, atrial fibrillation or heart
695 failure and 0 otherwise. The severity indicator was set equal to 1 for severe and severe with EOD
696 patients and 0 for Mild and Moderate COVID patients; mortality was set equal to 1 for deceased

patients and 0 otherwise. Significant association based on 95% confidence interval (CI) are reported in **Fig. 1c** and **Supplementary Table. 2**. CI of odds ratio were computed based on 1000 bootstrap iterations. At each bootstrap iteration, patients were sampled with replacements and logistic regressions were estimated considering as outcome severity and mortality. Then, 95% CI of coefficients and odds ratio were estimated across bootstrap iterations (**Fig. 1d**).

External Validation Cohort

For this analysis, we considered 228 patients with clinical data such as age, gender and GI symptoms. A multivariate logistic regression was utilized to model mortality, ICU admission and the composite outcome of ICU admission or mortality as function of presence or absence of diarrhea and clinical variables including age, gender, BMI, heart disease, COPD, diabetes and hypertension. Heart disease was set equal to 1 if the patient was either affected by coronary artery disease or atrial fibrillation and 0 otherwise. Confidence intervals of odds ratio were computed based on 1000 bootstrap iterations. At each bootstrap iteration, patients were sampled with replacements and logistic regressions were estimated considering the outcome as mortality, ICU admission or the composite outcome of ICU admission or death. Then, 95% confidence intervals of odds ratio were estimated across bootstrap iterations (**Fig. 1e**).

Predictive performance based on the Internal Validation Cohort

For this analysis, we considered 233 patients with clinical data including age, BMI, and GI symptoms. In order to evaluate the predictive performance of each model, bootstrapping was performed. Specifically, at each bootstrap iteration, we randomly sampled patients in the discovery cohort with replacement and estimated a logistic regression to model each outcome as function of a particular GI symptom, age and BMI. In this analysis, only age and BMI were adjusted for since they were the only variables significantly associated with both outcomes across different GI symptoms models in the discovery cohort (**Fig. 1c).** Then, the estimated model was utilized to predict the outcome of patients in the validation cohort. This procedure was repeated for 1000 bootstrap iterations. For each iteration, Receiving Operating Characteristic (ROC) curve and area under the curve (AUC) were computed. For comparison purposes, the distribution of AUC across 1000 bootstrap iterations from the predictive model based on age and BMI only was considered. **Fig. 1f** (left panel) shows the boxplot of AUC values across 1000 bootstrap iterations. Then, considering the following model

$$\text{outcome} = f(\text{age} + \text{bmi} + \text{any GI symptom}) \qquad \text{[Model 1]}$$

729 we evaluated the effect of each variable on the outcome by computing the reduction in AUC
730 obtained after removing one variable at a time. For this purpose, the AUC of model [Model 1] was
731 compared to the following three models

732 outcome = f(age + bmi) [Model 2]

733 outcome = f(age + any GI symptom) [Model 3]

734 outcome = f(bmi + any GI symptom) [Model 4]

735 for 1000 bootstrap iterations. Following the strategy above, at each bootstrap iteration, patients
736 were sampled with replacement. **Fig. 1f** (right panel) shows the 95% confidence intervals of
737 difference in AUC between [Model 1] and [Model 2], [Model 3] and [Model 4] (i.e., AUCModel1 -
738 AUCModel2, AUCModel1 - AUCModel3, AUCModel1 - AUCModel4) across 1000 bootstrap
739 iterations. The difference in AUC was computed considering both mortality and severity as the
740 outcome.

741

742 **ELLA Cytokine panel**

743 The ELLA platform is a method for rapid cytokine measurement using microfluidics ELISA assays.
744 The assay measured TNF-α, IL-6, IL-8, and IL-1β, previously validated by the Mount Sinai Human
745 Immune Monitoring Center (HIMC) using plasma from multiple myeloma patients and recently
746 reported for large cohort of COVID-19 patients admitted to Mount Sinai Hospital[35].

747

748 **Multiplexed proteomic assay (Olink)**

749 For analysis of circulating cytokines, we used a multiplexed proteomic inflammation panel
750 (Olink), which consists of 92 inflammation-related proteins quantified by an antibody-mediated
751 proximity extension-based assay[89]. Samples with normalized protein expression values below
752 the limit-of-detection in >75% of samples were excluded from further analysis. For the
753 remainder of analytes, any sample under the limit of detection was assigned a value of the limit-
754 of-detection divided by the square root of 2. The log2 fold-change over the median healthy
755 control protein expression was then calculated, and the Benjamini-Hochberg[90] procedure was
756 used to adjust P values for multiple testing

757

758 **Consensus Clustering of Olink Data**

759 For this analysis, we considered 238 samples with GI symptoms annotation. Consensus
760 clustering was performed based on the abundance of 92 cytokines across all 238 samples.
761 Consensus clustering was performed using the R packages ConsensusClusterPlus[91] based on
762 z-score normalized data. Specifically, markers were partitioned into six clusters using the Kaplan

763 Meier (KM) algorithm, which was repeated 1000 times. Then, markers in each cluster were
764 considered in order to derive cluster z-score signatures via package GSVA[92]. Based on these
765 signatures, the association between different clusters and GI symptoms were derived via logistic
766 regression with outcome corresponding to each GI symptom. **Fig. 2c** shows the signed FDR (-
767 log10 scale). P-values were adjusted via Benjamini-Hochberg[90].
768
769 **Defining associations between GI symptoms and Olink protein markers**
770 Associations between GI symptoms and Olink proteomic data were derived using unpaired t-test
771 comparing the symptomatic and asymptomatic groups. P-values were adjusted via Benjamini-
772 Hochberg[90]. Only associations passing a 10% FDR were reported as significant (**Fig. 2d**).
773
774 **Defining associations between GI symptoms and ELLA cytokine markers**
775 Unpaired t-test were used to compare individual cytokines quantified by the ELLA panel between
776 GI symptomatic and asymptomatic groups. P-values were adjusted via Benjamini-Hochberg[90].
777
778 **Biopsy collection and processing for Mass cytometry (CyTOF)**
779 Endoscopic biopsies were obtained from COVID-19 patients and non-COVID-19 controls during
780 clinically indicated endoscopic procedures. The biopsies were processed in biosafety level 3
781 (BSL-3) facility within 2 hours of collection.
782 Briefly, biopsies were transferred to 10 ml of 'dissociation buffer' (1M HEPES(Lonza), 5uM
783 EDTA(Invitrogen), 10% FBS in HBSS buffer (Gibco). The tubes were kept in a shaker (180 rpm,
784 37°C) for 20 min and then gently vortexed for 10 seconds. Cell suspensions were collected after
785 passing the biopsies through 100um cell strainers. A second round of EDTA dissociation was
786 performed as detailed above. The cell suspension was centrifuged at 1800 rpm for 10 min to pellet
787 the epithelial fraction and kept on ice. The 'non-epithelial fraction' of the tissue was transferred to
788 fresh tubes containing a 'digestion buffer' (2% FBS, 0.005g Collagenase type IV per sample
789 (Sigma), 100 ul DNAse-I(Sigma) in 10ml in RPMI). Tubes were placed in the shaker (180 rpm,
790 37°C) for 40 min and thereafter gently vortexed for 30 sec. The digested tissues were filtered
791 through 100 um cell strainers followed by a second round of filtration through 40um cell strainers.
792 Cell suspensions were centrifuged at 1800 rpm for 10 min to obtain lamina propria mononuclear
793 cells. Both epithelial cell (EC) and lamina propria (LP) pellets were then resuspended into 500ul
794 of RPMI (Gibco) containing 10% FBS+ 1μlRh103 +1μl IdU and incubated at 37°C for 20 min. 5
795 ml RPMI (+10%FBS) was added to each tube and spun at 1800 rpm to pellet cells. 700μl of Prot1
796 stabilizer (SmartTube Inc.) was added to each tube and transferred to cryovials and incubated at

797 room temperature for 10 min. Cryovials were immediately transferred to -80 until the sample was
798 acquired for mass cytometry as detailed below.
799
800 **Blood collection and processing for CyTOF**
801 Phlebotomy was performed on COVID-19 patients and non-COVID-19 controls at the time of
802 endoscopic evaluation. All the blood samples from COVID-19 patients were processed in
803 enhanced BSL2 conditions per institutional guidelines. Briefly, 15ml of Lymphosep® -
804 Lymphocyte Separation Medium (MP Bio.) was added to each 50 ml centrifugation tube. Blood
805 was diluted with PBS to bring the volume up to 30ml and diluted blood was layered gently over
806 Lymphosep®. Tubes were then centrifuged at 2000 rpm for 20 mins with the brakes and
807 acceleration off. After centrifugation, with a 3ml transfer pipet, the buffy coat containing PBMCs
808 was transferred to another 15ml Falcon tube and was centrifuged at 1800 rpm for 10 mins. Pellets
809 were resuspended in PBS and tubes were centrifuged at 1800 rpm for 10 mins. PBMC pellets
810 were resuspended in the freezing medium (10% DMSO + 44% FBS in RPMI) and cryopreserved
811 at -80 °C.
812
813 **CyTOF processing and data acquisition**
814 Cells were processed and as previously described[93] according to the manufacturer's instructions.
815 Briefly, EC and LP SmartTube proteomic stabilized samples were thawed in a 10°C water bath
816 and washed with Cell Staining Buffer (Fluidigm). To facilitate data acquisition and doublet
817 removal, multiple samples were also barcoded using Fluidigm Pd barcoding kits and then washed
818 and pooled for data acquisition. Immediately prior to data acquisition, samples were washed with
819 Cell Staining Buffer and Cell Acquisition Solution (Fluidigm) and resuspended at a concentration
820 of 1 million cells per ml in Cell Acquisition Solution containing a 1:20 dilution of EQ Normalization
821 beads (Fluidigm). The samples were then acquired on a Helios Mass Cytometer equipped with a
822 wide-bore sample injector at an event rate of <400 events per second. After acquisition, repeat
823 acquisitions of the same sample concatenated and normalized using the Fluidigm software, and
824 barcoded samples were de-multiplexed using the Zunder single cell debarcoder.
825
826 **CyTOF Data analysis**
827 De-barcoded files were uploaded to Cytobank for analyses. Immune cells were identified based
828 on Ir-193 DNA intensity and CD45 expression; Ce140+ normalization beads, CD45-low/Ir-193-
829 low debris and cross-sample and Gaussian ion-cloud multiplets were excluded from subsequent
830 downstream analysis. Major immune cell types were identified using automated Astrolabe

831 approach, the result of which largely correlated well with our manual gating approaches. The
832 impact of each tested condition on relative staining quality was evaluated in two ways: 1) overall
833 correlations were determined by calculating the Pearson's correlation coefficients for the median
834 expression of each marker across each defined immune subset; and 2) a staining index was
835 calculated using defined populations showing the highest and lowest expression levels of each
836 marker: SI = (Medianpos - Medianneg) / 2 X Std.Devneg. It is already shown that SmartTube-
837 based fixation protocols take into account previously described mass cytometry artifacts such as
838 cell-cell multiplets, isotopic spillover or oxidation, or mass cytometer instrument configuration[93].
839

840 **Statistical Analysis for CyTOF**

841 Pre-gated viable CD45+ cells were first clustered and annotated using the Astrolabe Cytometry
842 Platform (Astrolabe Diagnostics, Inc.), which involves using a hierarchy-based FlowSOM
843 algorithm for labeling cell populations in individual samples. These Astrolabe Profiling clusters
844 from each tissue type were then meta-clustered across all samples utilizing Clustergrammer2's
845 interactive heatmap as a method to interrogate antibody expression across every cluster and
846 curate and assign cell population categories. Single sample clusters were also visualized using
847 UMAP. Pairwise comparisons were performed on the frequencies of each identified cell
848 population between the patient cohorts (COVID-19 vs. control, COVID-19 severe vs. control,
849 COVID19-moderate vs. control) to determine fold change, p-values and FDR adjusted p-values
850 using the Benjamini-Hochberg[90] method to account for multiple comparisons.
851

852 **Cell Culture Experiments/ RNA isolation/ qPCR/Virus Isolation**

853 African green monkey kidney epithelial cells (Vero E6) were originally purchased from American
854 Type Culture Collection (ATCC). Cells were maintained in Dulbecco's modified Eagle's medium
855 (DMEM) w/ L-glutamate, sodium pyruvate (Corning) supplemented with 10% fetal bovine serum
856 (FBS), 100 U penicillin per ml, and 100 mg streptomycin per ml. For all experiments, the cells
857 were always maintained in monolayers.

858 Several attempts were made to isolate live infectious particles from these biopsies. Briefly,
859 biopsies were collected and stored in PBS until homogenization. Following homogenization and
860 centrifugation (10,000 × g, 20 min, 4°C), the resulting supernatant tissue supernatant was
861 inoculated onto Vero E6 monolayer maintained in optimal virus growth media for SARS-CoV-2
862 virus (DMEM w/ L-Glutamate, Sodium Pyruvate, 2% FBS, 100 U Penicillin/ml, and 100 mg
863 Streptomycin/ml, 10 mM Non-Essential Amino Acids, 1 mM Sodium Pyruvate and 10 mM

864 HEPES). Vero E6 cells were incubated at 37 °C, 5% CO2 for a week and monitored daily for
865 potential cytopathic effect (CPE).
866 Cell culture supernatants were also collected and assessed for presence of infective
867 particles by plaque assay. Briefly, ten-fold serial dilutions were performed in infection media for
868 SARS-CoV-2 and inoculated onto confluent Vero E6 cell monolayer in 6-well plate. After one-hour
869 adsorption, supernatants were removed, and cells monolayers were overlaid with minimum
870 essential media (MEM) containing 2% FBS and purified agar (OXOID) at a final concentration of
871 0.7%. Cells were then incubated 3 days at 37°C. Cells were fixed overnight with 10%
872 formaldehyde for inactivation of potential SARS CoV2 virus. Overlay was removed and cells were
873 washed once with PBS. A 2% crystal violet solution was used for plaque visualization and count.
874 Experiments were performed under BSL3 conditions.
875
876 **Specimen Processing for Nucleic Acid Extraction**
877 Whole biopsy tissues from COVID-19 patients and non COVID controls were directly
878 homogenized in Trizol (Invitrogen) and used to detect the presence of viral RNA. In parallel, RNA
879 isolated from epithelial compartment and lamina propria fractions from biopsies post-processing
880 were used for transcriptomics analyses. Total RNA was extracted using Direct-zol RNA Miniprep
881 Plus (Zymo) kit according to the manufacturer's instructions.
882
883 **RT-qPCR for Viral Determination**
884 RNA was retro-transcribed using the enzyme Maxima First Strand cDNA (Thermofisher), and
885 PCR reaction was performed using the TaqMan™ Universal PCR Master Mix (Thermofisher). For
886 detection of SARS-CoV-2 RNA, we used the following primers and probe targeting the N gene:
887 N1- SARS-CoV2-F5′GACCCCAAAATCAGCGAAAT;
888 N1-SARS-CoV2-R5'TCTGGTTACTGCCAGTTGAATCTG;
889 N1-SARS-CoV2-P FAM5' ACCCCGCATTACGTTTGGTGGACC-BHQ-1
890 (https://www.cdc.gov/coronavirus/2019-ncov/lab/rt-pcr-panel-primer-probes.html)
891 Another set of primers was included to detect host 18s and GADPH. Limit of detection and
892 amplification efficiency were calculated before GI tissue quantification for N1 (173%; R^2>0.94)
893 primers using plasmids expressing the NP protein (2019-nCoV_N_Positive Control, IDT, cat.
894 10006625). RNA from GI tissue were run in triplicate in 384 plates using the following cycling
895 conditions on the Roche LightCycler 480 Instrument II (Roche Molecular Systems, 05015243001):
896 50 C for 2 min; 95 C for 10 min; 40 cycles of 95C for 15 sec and 60 C for 1 min. Samples below
897 the limit of detection (Ct≥34 corresponding to 100 genome copies/reaction) were considered

898 negative. Primers and probes for housekeeping genes GAPDH (assay ID Hs02758991_g1 FAM)
899 and 18S (assay ID Hs03928990_g1 FAM) were obtained from Thermofisher Scientific).
900
901 **Cell Culture Experiments/ Virus Isolation**
902 African green monkey kidney epithelial cells (Vero E6) were originally purchased from American
903 Type Culture Collection (ATCC). Cells were maintained in Dulbecco's modified Eagle's medium
904 (DMEM) w/ L-glutamate, sodium pyruvate supplemented with 10% fetal bovine serum (FBS), 100
905 U penicillin per ml, and 100 mg streptomycin per ml. For all experiments, the cells were always
906 maintained in monolayers.
907 Several attempts were made to isolate live infectious particles from these biopsies. Briefly,
908 biopsies were collected and stored in PBS until homogenization. Following homogenization and
909 centrifugation (10,000 × g, 20 min, 4°C), the resulting supernatant tissue supernatant was
910 inoculated onto Vero E6 monolayer maintained in optimal virus growth media for SARS-CoV-2
911 virus (DMEM w/ L-Glutamate, Sodium Pyruvate, 2% FBS, 100 U Penicillin/ml, and 100 mg
912 Streptomycin/ml, 10 mM Non-Essential Amino Acids, 1 mM Sodium Pyruvate and 10 mM
913 HEPES). Vero E6 cells were incubated at 37 °C, 5% CO2 for a week and monitored daily for
914 potential cytopathic effect (CPE).
915 Cell culture supernatants were also collected and assessed for presence of infective
916 particles by plaque assay. Briefly, ten-fold serial dilutions were performed in infection media for
917 SARS-CoV-2 and inoculated onto confluent Vero E6 cell monolayer in 6-well plate. After one-hour
918 adsorption, supernatants were removed, and cells monolayers were overlaid with minimum
919 essential media (MEM) containing 2% FBS and purified agar (OXOID) at a final concentration of
920 0.7%. Cells were then incubated 3 days at 37°C. Cells were fixed overnight with 10%
921 formaldehyde for inactivation of potential SARS CoV2 virus. Overlay was removed and cells were
922 washed once with PBS. A 2% crystal violet solution was used for plaque visualization and count.
923 Experiments were performed under BSL3 conditions.
924
925 **RNA Sequencing**
926
927 *Library preparation and sequencing*
928 RNA-sequencing (RNA-seq) was performed on tissue biopsies from paired EC and LP samples
929 from COVID-19 cases and controls. Directional RNA-seq libraries were prepared from 50 ng of
930 total RNA with the TruSeq® Stranded Total RNA prep with Ribo-Zero kit (cat no. 20020599).

931 Paired-end (100 bp) sequencing was performed for DNA libraries on an Illumina NovaSeq
932 instrument on a NovaSeq S1 Flowcell, with an average yield of 39 million PE reads/sample.
933
934 *RNA-seq analysis*
935 Base-calling and quality scoring of sequencing data were done through Illumina's Real-Time
936 Analysis (RTA) software. RNA-seq data processing and reference mapping were done with
937 custom analysis scripts combining publicly available tools as previously described[94] with
938 modifications as follows, reads were mapped to a custom reference that combined the human
939 hg38 reference genome (Release 34, GRCh38.p13) and the SARS-CoV-2 genome (RefSeq
940 NC_045512) for simultaneous quantification of host and virus transcripts.
941 Differential gene expression (DGE) analysis was performed with the Bioconductor edgeR
942 package [95] using as input a combined matrix of mapped paired-end read raw counts, with genes
943 in rows and samples in columns. Prior to DEG analysis, gene counts were converted to fragments
944 per kb per million reads (FPKM) with the RSEM package with default settings in strand-specific
945 mode[96].
946 Genes with less than 1 FPKM in at least 50% of the samples were removed. The remaining
947 gene counts were then normalized across samples using the weighted trimmed mean of M-values
948 (TMM) method[97].The dispersion was estimated by fitting a generalized linear model (GLM) as
949 implemented in edgeR, sex was fitted as a covariate on a per-patient paired design. Pairwise
950 comparisons were performed between sample groups (i.e., between tissue sections, and between
951 cases and controls). Significant expression differences were selected based on eBayes adjusted
952 p values corrected for multiple testing using the Benjamini-Hochberg method ($q \leq 0.05$).
953
954 *Gene Ontology and Pathway Enrichment Analysis*
955 KEGG pathway and gene ontology (GO) biological process (BP), molecular function (MF), and/or
956 cellular component (CC) enrichment analyses were performed using the gProfileR R v0.6.8
957 package[98]. The background gene set was restricted genes with detected expression (defined as
958 genes with expression levels above 1 FPKM in at least 50% of samples). Genes with differential
959 expression were ranked by log 2 fold change and used as an ordered query. P values were
960 corrected using the g:SCS algorithm to account for multiple comparisons.
961
962 *Cell-type deconvolution and gene signature enrichment analysis*
963 For cell-type deconvolution of the bulk RNA-seq data, gene set enrichment analysis of
964 differentially expressed genes of cases vs controls comparisons was performed against cell type

965 gene-expression single-cell signatures from intestinal mucosa[46] and dendritic cell (DCs) subsets
966 gene-expression signatures from ileum[45]. Similarly, differentially expressed genes were tested for
967 enrichment of gene signatures associated with an antiviral response, inflammation, and cytokine
968 signaling in acutely infected post-mortem tissue with SARS-CoV-2[30] , were tested for significant
969 ($p \leq 0.05$) enrichment using Fisher's exact tests and using Bonferroni correction for multiple
970 comparisons.
971 Additionally, Geneset enrichment analysis (GSEA)[99] was carried out on a rank ordered list
972 of the infected EC versus control molecular analysis. The ranking metric used was logFC * -logP
973 value, however, the results were similar when logFC metric was also used (data not shown). For
974 the COVID-19 associated datasets we curated two signatures from infected organoids[100]: hSIOs-
975 COVID-19: human small intestinal organoids (hSIOs) grown in either i) Wnt high expansion (EXP)
976 medium (at adjP<0.05) or ii) differentiation (DIF) medium (at adjP<0.1). The standard GSEA
977 settings were used, namely 'meandiv' for normalization mode, 'weighted' enrichment statistic, and
978 '1000' permutations. GSEA using the Hallmark database (v7.1, [101]) was also performed with the
979 same settings.
980
981 **Immunofluorescent (IF) microscopy**
982 Formalin fixed, paraffin embedded tissue acquired during routine clinical care was obtained from
983 the pathology core at our institution. Sections (5μm) were dewaxed in xylene and rehydrated in
984 graded alcohol and then phosphate-buffered saline (PBS). Heat-induced epitope retrieval was
985 performed by incubating slides in a pressure cooker for 15 minutes on high in target retrieval
986 solution (Dako, S1699). Slides were then left to cool in the solution at room temperature for 30
987 minutes. Slides were washed twice in PBS and then permeabilized for 30 minutes in 0.1% tritonX-
988 100 in PBS. Non-specific binding was blocked with 10% goat serum for 1 hour at room
989 temperature. Sections were then incubated in primary antibodies diluted in blocking solution
990 overnight at 4°C. Primary and secondary antibodies are summarized in **Supplementary Table**
991 **11**. Slides were washed in PBST (0.1% tween 20, PBS) 3 times and then incubated in secondary
992 antibody and 4′,6-diamidino-2-phenylindole (1ug/mL) for 1 hour at room temperature. Sections
993 were washed twice in PBST and once in PBS then mounted with Fluoromount-G (Electron
994 microscopy sciences, 1798425). Controls included, omitting primary antibody (no primary
995 control), or substituting primary antibodies with non-reactive antibodies of the same isotype
996 (isotype control). Tissue was visualized and imaged using a Nikon Eclipse Ni microscope and
997 digital SLR camera (Nikon, DS-Qi2).
998

999 **Electron Microscopy (EM)**

1000 Biopsy specimens for electron microscopy were placed in 3% buffered glutaraldehyde. Following
1001 post-fixation in 1% osmium tetroxide, tissues were serially dehydrated and embedded in epoxy
1002 resin in standard fashion. One-micron toluidine-stained scout sections were prepared for light
1003 microscopic orientation; 80nm ultrathin sections for EM were stained with uranyl acetate and lead
1004 citrate and examined in a Hitachi 7650 transmission electron microscope at 80kV.

1005

1006 **Acknowledgements**

1007 We would like to thank the clinical staff, physicians and patients who participated in this study.
1008 This research was partly funded by NIH/NIDDK123749 (SM). Additional support was provided by
1009 CRIP (Center for Research for Influenza Pathogenesis), a NIAID supported Center of Excellence
1010 for Influenza Research and Surveillance (CEIRS, contract # HHSN272201400008C), and NIAID
1011 R01AI113186 (to H.B). Additionally, the work was supported by the generous support of the JPB
1012 Foundation, the Open Philanthropy Project (research grant 2020-215611 (5384)), the Defense
1013 Advanced Research Projects Agency, and anonymous donors to AG-S. MT was funded by the
1014 Digestive Disease Research Foundation (DDRF). A.S.G-R. is supported in part by a Robin
1015 Chemers Neustein Postdoctoral Fellowship Award. The research carried out by H.V.B and A.S.G-
1016 R was supported by the Office of Research Infrastructure of the National Institutes of Health (NIH)
1017 under awards S10OD018522 and S10OD026880. S.T.C. is supported by grant F30CA243210.
1018 G.J.B. is supported by a Research Fellowship Award from the Crohn's and Colitis Foundation of
1019 America. M.P.S. is supported by NIH T32 5T32AI007605. S.G. is supported by grants U24
1020 CA224319, U01 DK124165, and P01 CA190174. We also thank Randy Albrecht for support with
1021 the BSL3 facility and procedures at the Icahn School of Medicine at Mount Sinai (ISMMS).

1022

1023

1024 **References**

1025

1026 1. Zhu, N.*, et al.* A Novel Coronavirus from Patients with Pneumonia in China, 2019. *N Engl*
1027 *J Med* **382**, 727-733 (2020).
1028 2. Wang, C., Horby, P.W., Hayden, F.G. & Gao, G.F. A novel coronavirus outbreak of global
1029 health concern. *Lancet* **395**, 470-473 (2020).
1030 3. Huang, C.*, et al.* Clinical features of patients infected with 2019 novel coronavirus in
1031 Wuhan, China. *Lancet* **395**, 497-506 (2020).
1032 4. Goyal, P.*, et al.* Clinical Characteristics of Covid-19 in New York City. *N Engl J Med* **382**,
1033 2372-2374 (2020).

1034 5. Xu, T., *et al.* Epidemiological and clinical features of asymptomatic patients with SARS-
1035 CoV-2 infection. *J Med Virol* (2020).
1036 6. Coronavirus Disease 2019 (COVID-19): Symptoms of Coronavirus: Centers for Disease
1037 Control and Prevention, 2020. https://www.cdc.gov/coronavirus/2019-ncov/symptoms-
1038 testing/symptoms.html. Last updated May 13, 2020.
1039 7. Jin, X., *et al.* Epidemiological, clinical and virological characteristics of 74 cases of
1040 coronavirus-infected disease 2019 (COVID-19) with gastrointestinal symptoms. *Gut* **69**,
1041 1002-1009 (2020).
1042 8. Pan, L., *et al.* Clinical Characteristics of COVID-19 Patients With Digestive Symptoms in
1043 Hubei, China: A Descriptive, Cross-Sectional, Multicenter Study. *Am J Gastroenterol* **115**,
1044 766-773 (2020).
1045 9. Gupta, A., *et al.* Extrapulmonary manifestations of COVID-19. *Nat Med* **26**, 1017-1032
1046 (2020).
1047 10. Tian, Y., Rong, L., Nian, W. & He, Y. Review article: gastrointestinal features in COVID-19
1048 and the possibility of faecal transmission. *Aliment Pharmacol Ther* **51**, 843-851 (2020).
1049 11. Cheung, K.S., *et al.* Gastrointestinal Manifestations of SARS-CoV-2 Infection and Virus
1050 Load in Fecal Samples From a Hong Kong Cohort: Systematic Review and Meta-analysis.
1051 *Gastroenterology* **159**, 81-95 (2020).
1052 12. Harmer, D., Gilbert, M., Borman, R. & Clark, K.L. Quantitative mRNA expression profiling
1053 of ACE 2, a novel homologue of angiotensin converting enzyme. *FEBS Lett* **532**, 107-110
1054 (2002).
1055 13. Suárez-Fariñas, M., *et al.* Intestinal inflammation modulates the expression of ACE2 and
1056 TMPRSS2 and potentially overlaps with the pathogenesis of SARS-CoV-2 related disease.
1057 *bioRxiv*, 2020.2005.2021.109124 (2020).
1058 14. Young, B.E., *et al.* Epidemiologic Features and Clinical Course of Patients Infected with
1059 SARS-CoV-2 in Singapore. *JAMA - Journal of the American Medical Association* (2020).
1060 15. Xiao, F., *et al.* Evidence for Gastrointestinal Infection of SARS-CoV-2. *Gastroenterology*
1061 **158**, 1831-1833 e1833 (2020).
1062 16. Holshue, M.L., *et al.* First Case of 2019 Novel Coronavirus in the United States. *N Engl J*
1063 *Med* **382**, 929-936 (2020).
1064 17. Wu, Y., *et al.* Prolonged presence of SARS-CoV-2 viral RNA in faecal samples. *Lancet*
1065 *Gastroenterol Hepatol* **5**, 434-435 (2020).
1066 18. Fehr, A.R. & Perlman, S. Coronaviruses: An overview of their replication and
1067 pathogenesis. (2015).
1068 19. Leung, W.K., *et al.* Enteric involvement of severe acute respiratory syndrome-associated
1069 coronavirus infection. *Gastroenterology* **125**, 1011-1017 (2003).
1070 20. Chan, K.H., *et al.* Detection of SARS coronavirus in patients with suspected SARS. *Emerg*
1071 *Infect Dis* **10**, 294-299 (2004).
1072 21. Assiri, A., *et al.* Epidemiological, demographic, and clinical characteristics of 47 cases of
1073 Middle East respiratory syndrome coronavirus disease from Saudi Arabia: a descriptive
1074 study. *Lancet Infect Dis* **13**, 752-761 (2013).
1075 22. Corman, V.M., *et al.* Detection of 2019 novel coronavirus (2019-nCoV) by real-time RT-
1076 PCR. *Euro Surveill* **25**(2020).

1077 23. Wang, X.*, et al.* Aberrant gut microbiota alters host metabolome and impacts renal
1078 failure in humans and rodents. *Gut* (2020).
1079 24. Sultan, S.*, et al.* AGA Institute Rapid Review of the GI and Liver Manifestations of COVID-
1080 19, Meta-Analysis of International Data, and Recommendations for the Consultative
1081 Management of Patients with COVID-19. *Gastroenterology* (2020).
1082 25. Munster, V.J.*, et al.* Respiratory disease in rhesus macaques inoculated with SARS-CoV-
1083 2. *Nature* (2020).
1084 26. Bojkova, D.*, et al.* Proteomics of SARS-CoV-2-infected host cells reveals therapy targets.
1085 *Nature* (2020).
1086 27. Zang, R.*, et al.* TMPRSS2 and TMPRSS4 promote SARS-CoV-2 infection of human small
1087 intestinal enterocytes. *Sci Immunol* **5**(2020).
1088 28. Zhou, J.*, et al.* Infection of bat and human intestinal organoids by SARS-CoV-2. *Nat Med*
1089 (2020).
1090 29. Lamers, M.M.*, et al.* SARS-CoV-2 productively infects human gut enterocytes. *Science*
1091 (2020).
1092 30. Blanco-Melo, D.*, et al.* Imbalanced Host Response to SARS-CoV-2 Drives Development of
1093 COVID-19. *Cell* **181**, 1036-1045 e1039 (2020).
1094 31. Lucas, C.*, et al.* Longitudinal analyses reveal immunological misfiring in severe COVID-19.
1095 *Nature* **584**, 463-469 (2020).
1096 32. Xu, X.*, et al.* Analysis of inflammatory parameters and disease severity for 88
1097 hospitalized COVID-19 patients in Wuhan, China. *Int J Med Sci* **17**, 2052-2062 (2020).
1098 33. Liu, Z.*, et al.* Dynamic Interleukin-6 Level Changes as a Prognostic Indicator in Patients
1099 With COVID-19. *Front Pharmacol* **11**, 1093 (2020).
1100 34. Akbari, H.*, et al.* The role of cytokine profile and lymphocyte subsets in the severity of
1101 coronavirus disease 2019 (COVID-19): A systematic review and meta-analysis. *Life Sci*
1102 **258**, 118167 (2020).
1103 35. Del Valle, D.M.*, et al.* An inflammatory cytokine signature helps predict COVID-19
1104 severity and death. *medRxiv* (2020).
1105 36. Laing, A.G.*, et al.* A dynamic COVID-19 immune signature includes associations with
1106 poor prognosis. *Nat Med* (2020).
1107 37. Mathew, D.*, et al.* Deep immune profiling of COVID-19 patients reveals distinct
1108 immunotypes with therapeutic implications. *Science* (2020).
1109 38. Liu, J.*, et al.* Longitudinal characteristics of lymphocyte responses and cytokine profiles
1110 in the peripheral blood of SARS-CoV-2 infected patients. *EBioMedicine* **55**, 102763
1111 (2020).
1112 39. Arunachalam, P.S.*, et al.* Systems biological assessment of immunity to mild versus
1113 severe COVID-19 infection in humans. *Science* (2020).
1114 40. Richardson, S.*, et al.* Presenting Characteristics, Comorbidities, and Outcomes Among
1115 5700 Patients Hospitalized With COVID-19 in the New York City Area. *JAMA* (2020).
1116 41. Team, C.C.-R. Severe Outcomes Among Patients with Coronavirus Disease 2019 (COVID-
1117 19) - United States, February 12-March 16, 2020. *MMWR Morb Mortal Wkly Rep* **69**,
1118 343-346 (2020).
1119 42. Falschlehner, C., Schaefer, U. & Walczak, H. Following TRAIL's path in the immune
1120 system. *Immunology* **127**, 145-154 (2009).

1121 43. Chyuan, I.T., Tsai, H.F., Wu, C.S., Sung, C.C. & Hsu, P.N. TRAIL-Mediated Suppression of T
1122 Cell Receptor Signaling Inhibits T Cell Activation and Inflammation in Experimental
1123 Autoimmune Encephalomyelitis. *Front Immunol* **9**, 15 (2018).
1124 44. Mackall, C.L., Fry, T.J. & Gress, R.E. Harnessing the biology of IL-7 for therapeutic
1125 application. *Nat Rev Immunol* **11**, 330-342 (2011).
1126 45. Martin, J.C.*, et al.* Single-Cell Analysis of Crohn's Disease Lesions Identifies a Pathogenic
1127 Cellular Module Associated with Resistance to Anti-TNF Therapy. *Cell* **178**, 1493-1508
1128 e1420 (2019).
1129 46. Smillie, C.S.*, et al.* Intra- and Inter-cellular Rewiring of the Human Colon during
1130 Ulcerative Colitis. *Cell* **178**, 714-730 e722 (2019).
1131 47. Kotarsky, K.*, et al.* A novel role for constitutively expressed epithelial-derived
1132 chemokines as antibacterial peptides in the intestinal mucosa. *Mucosal Immunol* **3**, 40-
1133 48 (2010).
1134 48. Hamming, I.*, et al.* Tissue distribution of ACE2 protein, the functional receptor for SARS
1135 coronavirus. A first step in understanding SARS pathogenesis. *Journal of Pathology*
1136 (2004).
1137 49. Li, M.Y., Li, L., Zhang, Y. & Wang, X.S. Expression of the SARS-CoV-2 cell receptor gene
1138 ACE2 in a wide variety of human tissues. *Infect Dis Poverty* **9**, 45 (2020).
1139 50. Nobel, Y.R.*, et al.* Gastrointestinal Symptoms and Coronavirus Disease 2019: A Case-
1140 Control Study From the United States. *Gastroenterology* **159**, 373-375 e372 (2020).
1141 51. Blumfield, E. & Levin, T.L. COVID-19 in pediatric patients: a case series from the Bronx,
1142 NY. *Pediatr Radiol* (2020).
1143 52. Blumfield, E., Levin, T.L., Kurian, J., Lee, E.Y. & Liszewski, M.C. Imaging Findings in
1144 Multisystem Inflammatory Syndrome in Children (MIS-C) Associated with COVID. *AJR*
1145 *Am J Roentgenol* (2020).
1146 53. Aghemo, A.*, et al.* COVID-19 Digestive System Involvement and Clinical Outcomes in a
1147 Large Academic Hospital in Milan, Italy. *Clin Gastroenterol Hepatol* (2020).
1148 54. Lin, L.*, et al.* Gastrointestinal symptoms of 95 cases with SARS-CoV-2 infection. *Gut* **69**,
1149 997-1001 (2020).
1150 55. Mehta, P.*, et al.* COVID-19: consider cytokine storm syndromes and
1151 immunosuppression. *Lancet* **395**, 1033-1034 (2020).
1152 56. Cao, W.*, et al.* High-Dose Intravenous Immunoglobulin as a Therapeutic Option for
1153 Deteriorating Patients With Coronavirus Disease 2019. *Open Forum Infect Dis* **7**, ofaa102
1154 (2020).
1155 57. Cavalli, G.*, et al.* Interleukin-1 blockade with high-dose anakinra in patients with COVID-
1156 19, acute respiratory distress syndrome, and hyperinflammation: a retrospective cohort
1157 study. *Lancet Rheumatol* **2**, e325-e331 (2020).
1158 58. Guo, Y.-R.*, et al.* The origin, transmission and clinical therapies on coronavirus disease
1159 2019 (COVID-19) outbreak – an update on the status. *Military Medical Research* (2020).
1160 59. Ackermann, M.*, et al.* Pulmonary Vascular Endothelialitis, Thrombosis, and Angiogenesis
1161 in Covid-19. *N Engl J Med* **383**, 120-128 (2020).
1162 60. Zhang, H.*, et al.* Histopathologic Changes and SARS-CoV-2 Immunostaining in the Lung of
1163 a Patient With COVID-19. *Ann Intern Med* **172**, 629-632 (2020).

1164 61. Cheng, Y.*, et al.* Kidney disease is associated with in-hospital death of patients with
1165 COVID-19. *Kidney Int* **97**, 829-838 (2020).
1166 62. Gabarre, P.*, et al.* Acute kidney injury in critically ill patients with COVID-19. *Intensive*
1167 *Care Med* **46**, 1339-1348 (2020).
1168 63. Varga, Z.*, et al.* Endothelial cell infection and endotheliitis in COVID-19. *Lancet* **395**,
1169 1417-1418 (2020).
1170 64. Liao, M.*, et al.* Single-cell landscape of bronchoalveolar immune cells in patients with
1171 COVID-19. *Nat Med* **26**, 842-844 (2020).
1172 65. Bradley, B.T.*, et al.* Histopathology and ultrastructural findings of fatal COVID-19
1173 infections in Washington State: a case series. *Lancet* **396**, 320-332 (2020).
1174 66. Gaffen, S.L. Structure and signalling in the IL-17 receptor family. *Nat Rev Immunol* **9**,
1175 556-567 (2009).
1176 67. Miossec, P. & Kolls, J.K. Targeting IL-17 and TH17 cells in chronic inflammation. *Nat Rev*
1177 *Drug Discov* **11**, 763-776 (2012).
1178 68. Wu, D. & Yang, X.O. TH17 responses in cytokine storm of COVID-19: An emerging target
1179 of JAK2 inhibitor Fedratinib. *J Microbiol Immunol Infect* **53**, 368-370 (2020).
1180 69. Josset, L.*, et al.* Cell host response to infection with novel human coronavirus EMC
1181 predicts potential antivirals and important differences with SARS coronavirus. *mBio* **4**,
1182 e00165-00113 (2013).
1183 70. Faure, E.*, et al.* Distinct immune response in two MERS-CoV-infected patients: can we go
1184 from bench to bedside? *PLoS One* **9**, e88716 (2014).
1185 71. Ramirez-Carrozzi, V.*, et al.* IL-17C regulates the innate immune function of epithelial
1186 cells in an autocrine manner. *Nat Immunol* **12**, 1159-1166 (2011).
1187 72. Pan, J.*, et al.* A novel chemokine ligand for CCR10 and CCR3 expressed by epithelial cells
1188 in mucosal tissues. *J Immunol* **165**, 2943-2949 (2000).
1189 73. Girard, D., Paquet, M.E., Paquin, R. & Beaulieu, A.D. Differential effects of interleukin-15
1190 (IL-15) and IL-2 on human neutrophils: modulation of phagocytosis, cytoskeleton
1191 rearrangement, gene expression, and apoptosis by IL-15. *Blood* **88**, 3176-3184 (1996).
1192 74. Regamey, N.*, et al.* Airway epithelial IL-15 transforms monocytes into dendritic cells. *Am*
1193 *J Respir Cell Mol Biol* **37**, 75-84 (2007).
1194 75. Mattei, F., Schiavoni, G., Belardelli, F. & Tough, D.F. IL-15 is expressed by dendritic cells
1195 in response to type I IFN, double-stranded RNA, or lipopolysaccharide and promotes
1196 dendritic cell activation. *J Immunol* **167**, 1179-1187 (2001).
1197 76. Rojas, J.M., Avia, M., Martin, V. & Sevilla, N. IL-10: A Multifunctional Cytokine in Viral
1198 Infections. *J Immunol Res* **2017**, 6104054 (2017).
1199 77. Han, H.*, et al.* Profiling serum cytokines in COVID-19 patients reveals IL-6 and IL-10 are
1200 disease severity predictors. *Emerg Microbes Infect* **9**, 1123-1130 (2020).
1201 78. Diao, B.*, et al.* Reduction and Functional Exhaustion of T Cells in Patients With
1202 Coronavirus Disease 2019 (COVID-19). *Front Immunol* **11**, 827 (2020).
1203 79. Laterre, P.F.*, et al.* Association of Interleukin 7 Immunotherapy With Lymphocyte Counts
1204 Among Patients With Severe Coronavirus Disease 2019 (COVID-19). *JAMA Netw Open* **3**,
1205 e2016485 (2020).
1206 80. Strater, J.*, et al.* TRAIL and its receptors in the colonic epithelium: a putative role in the
1207 defense of viral infections. *Gastroenterology* **122**, 659-666 (2002).

1208 81. Shi, H.*, et al.* Neutrophil calprotectin identifies severe pulmonary disease in COVID-19.
1209 *medRxiv* (2020).
1210 82. Chu, H.*, et al.* Comparative replication and immune activation profiles of SARS-CoV-2
1211 and SARS-CoV in human lungs: an ex vivo study with implications for the pathogenesis
1212 of COVID-19. *Clin Infect Dis* (2020).
1213 83. Bost, P.*, et al.* Host-Viral Infection Maps Reveal Signatures of Severe COVID-19 Patients.
1214 *Cell* **181**, 1475-1488 e1412 (2020).
1215 84. Chen, L.*, et al.* Elevated serum levels of S100A8/A9 and HMGB1 at hospital admission
1216 are correlated with inferior clinical outcomes in COVID-19 patients. *Cell Mol Immunol*
1217 (2020).
1218 85. Pelaseyed, T.*, et al.* The mucus and mucins of the goblet cells and enterocytes provide
1219 the first defense line of the gastrointestinal tract and interact with the immune system.
1220 *Immunol Rev* **260**, 8-20 (2014).
1221 86. Strober, W. & Fuss, I.J. Proinflammatory cytokines in the pathogenesis of inflammatory
1222 bowel diseases. *Gastroenterology* **140**, 1756-1767 (2011).
1223 87. Strober, W., Fuss, I.J. & Blumberg, R.S. The immunology of mucosal models of
1224 inflammation. *Annu Rev Immunol* **20**, 495-549 (2002).
1225 88. Chistiakov, D.A., Bobryshev, Y.V., Kozarov, E., Sobenin, I.A. & Orekhov, A.N. Intestinal
1226 mucosal tolerance and impact of gut microbiota to mucosal tolerance. *Front Microbiol* **5**,
1227 781 (2014).
1228 89. Gruber, C.*, et al.* Mapping Systemic Inflammation and Antibody Responses in
1229 Multisystem Inflammatory Syndrome in Children (MIS-C). *medRxiv* (2020).
1230 90. Benjamini, Y. & Hochberg, Y. Controlling the False Discovery Rate: A Practical and
1231 Powerful Approach to Multiple Testing. *Journal of the Royal Statistical Society. Series B*
1232 *(Methodological)* **57**, 289-300 (1995).
1233 91. Wilkerson, M.D. & Hayes, D.N. ConsensusClusterPlus: a class discovery tool with
1234 confidence assessments and item tracking. *Bioinformatics* **26**, 1572-1573 (2010).
1235 92. Hanzelmann, S., Castelo, R. & Guinney, J. GSVA: gene set variation analysis for
1236 microarray and RNA-seq data. *BMC Bioinformatics* **14**, 7 (2013).
1237 93. Geanon, D.*, et al.* A Streamlined CyTOF Workflow To Facilitate Standardized Multi-Site
1238 Immune Profiling of COVID-19 Patients. *medRxiv* (2020).
1239 94. Holmes, G.*, et al.* Integrated Transcriptome and Network Analysis Reveals
1240 Spatiotemporal Dynamics of Calvarial Suturogenesis. *Cell Rep* **32**, 107871 (2020).
1241 95. Robinson, M.D., McCarthy, D.J. & Smyth, G.K. edgeR: a Bioconductor package for
1242 differential expression analysis of digital gene expression data. *Bioinformatics* **26**, 139-
1243 140 (2010).
1244 96. Li, B. & Dewey, C.N. RSEM: accurate transcript quantification from RNA-Seq data with or
1245 without a reference genome. *BMC Bioinformatics* **12**, 323 (2011).
1246 97. Robinson, M.D. & Oshlack, A. A scaling normalization method for differential expression
1247 analysis of RNA-seq data. *Genome Biol* **11**, R25 (2010).
1248 98. Reimand, J., Kull, M., Peterson, H., Hansen, J. & Vilo, J. g:Profiler--a web-based toolset
1249 for functional profiling of gene lists from large-scale experiments. *Nucleic Acids Res* **35**,
1250 W193-200 (2007).

1251 99. Subramanian, A.*, et al.* Gene set enrichment analysis: a knowledge-based approach for
1252 interpreting genome-wide expression profiles. *Proc Natl Acad Sci U S A* **102**, 15545-
1253 15550 (2005).
1254 100. Lamers, M.M.*, et al.* SARS-CoV-2 productively infects human gut enterocytes. *Science*
1255 **369**, 50-54 (2020).
1256 101. Liberzon, A.*, et al.* The Molecular Signatures Database (MSigDB) hallmark gene set
1257 collection. *Cell Syst* **1**, 417-425 (2015).
1258

Table 1: Basic demographics and clinical characteristics in patients with and without GI symptoms. Number patients (%). For age, an unpaired t-test was performed. For categorical variables, the Fisher's exact test or the Chi-square test was used as appropriate.

	Total (n=634)	**GI symptoms (n=299)**	**No GI symptoms (n=335)**	**p-value**
Age (years)	64.0 ± 15.7	60.5 ± 15.0	67.2 ± 15.7	**<0.0001**
Male	369 ± 58.2	168 ± 56.2	201 ± 60.0	0.33
Race/ethnicities				
Hispanic	177 ± 27.9	85 ± 28.4	92 ± 27.5	
African-American	161 ± 25.4	66 ± 22.1	95 ± 28.4	
White	137 ± 21.6	70 ± 23.4	67 ± 20.0	
Asian	35 ± 5.5	22 ± 7.4	13 ± 3.9	
Other	124 ± 19.6	56 ± 18.7	68 ± 20.3	0.13
Comorbidities				
HTN	229 ± 36.1	112 ± 37.5	117 ± 34.9	0.51
Diabetes	141 ± 22.2	58 ± 19.4	83 ± 24.8	0.13
Obesity (BMI>30)*	211 ± 37.1	108 ± 40.6	103 ± 34.1	0.12
Chronic lung disease	59 ± 9.3	34 ± 11.4	25 ± 7.5	0.10
Heart disease	111 ± 17.5	48 ± 16.1	63 ± 18.8	0.40
Chronic kidney disease	95 ± 15.0	41 ± 13.7	54 ± 16.1	0.44
Cancer	66 ± 10.4	27 ± 9.0	39 ± 11.6	0.30
HIV	11 ± 1.7	5 ± 1.7	6 ± 1.8	0.99
IBD	7 ± 1.1	4 ± 1.3	3 ± 0.9	0.71

*BMI information available on only 568 patients

Table 2: Disease severity and clinical outcomes in those with and without GI symptoms. The Fisher's exact test or the Chi-square test was used as appropriate.

Disease severity	**Total (n=634)**	**GI symptoms (n=299)**	**No GI symptoms (n=335)**	**p-value**
Mild	54 ± 8.5	31 ± 10.4	23 ± 6.9	
Moderate	361 ± 56.9	188 ± 62.9	173 ± 51.6	
Severe	158 ± 24.9	63 ± 21.1	95 ± 28.4	
Severe with EOD	61 ± 9.6	17 ± 5.7	44 ± 13.1	**0.0004**
ICU admission	110 ± 17.4	45 ± 15.1	65 ± 19.4	0.17
Mortality	151 ± 23.8	47 ± 15.7	104 ± 31.0	**<0.0001**

Table 3: Proportion of patients with GI symptoms

GI symptom	Number patients (%)
Nausea	157 ± 24.8
Vomiting	82 ± 12.9
Diarrhea	245 ± 38.6
Any GI symptom	299 ± 47.2

Table 4: Basic demographics in survivors and non-survivors. For age, an unpaired t-test was performed. For categorical variables, the Fisher's exact test or the Chi-square test was used as appropriate.

	Total (n=634)	**Survivors (n=483)**	**Non-survivors (n=151)**	**p-value**
Age (years)	64.0 ± 15.7	61.3 ± 15.2	72.6 ± 14.1	**<0.0001**
Male	369 (58.2)	287 (59.4)	82 (54.3)	0.30
Disease severity				
Mild	54 ± 8.5	48 ± 9.9	6 ± 4.0	
Moderate	361 ± 56.9	318 ± 65.8	43 ± 28.5	
Severe	158 ± 24.9	95 ± 19.7	63 ± 41.7	
Severe with EOD	61 ± 9.6	22 ± 4.6	39 ± 25.8	**<0.0001**

1413 **Table 5:** Age, gender and mortality in an external validation (Italian) cohort stratified by presence or
1414 absence of diarrhea on admission. For age, an unpaired t-test was performed. For categorical variables,
1415 the Fisher's exact test or the Chi-square test was used as appropriate.
1416

	Total (n=287)	**Diarrhea on admission (n=80)**	**No diarrhea on admission (n=207)**	**p-value**
Age (years)	64.2 ± 13.6	60.6 ± 13.9	65.5 ± 13.3	**0.0056**
Male	195 ± 67.9	46 ± 57.5	149 ± 72.0	**0.0238**
ICU admission	52 ± 18.1	9 ± 11.3	43 ± 20.8	0.06
Mortality	57 ± 19.9	8 ± 10.0	49 ± 23.7	**0.008**
Death or ICU admission	99 ± 34.5	16 ± 20.0	83 ± 40.1	**0.0014**

1417
1418
1419
1420
1421
1422
1423
1424
1425
1426
1427

Table 6: Clinical characteristics of patients who underwent endoscopic GI biopsies

Patient #	Age*	Sex	Procedure	Tissue sample location	COVID-19 Antibody	Days from symptom onset (or first SARS-CoV-2 PCR if asymptomatic) to procedure	Days from last positive SARS-CoV-2 PCR to procedure (0 if positive swab after procedure)	COVID severity on admission
1	60-65	M	EGD	Duodenum	NA	10	10	Severe with EOD
2	5-10	M	EGD & colonoscopy	Intestinal Transplant	Positive	23	0	Severe
3	75-80	M	EGD	Duodenum	NA	25	9	Mild
4	30-35	F	EGD	Duodenum	NA	44	31	Severe with EOD
5	60-65	M	EGD	Duodenum	Positive	24	NA	Moderate
6	50-55	M	EGD	Duodenum	Positive	11	0	Asymptomatic / mild
7	55-60	M	EGD	Duodenum	Positive	19	19	Asymptomatic / mild
8	65-70	F	EGD	Duodenum	Positive	30	23	Severe
9	75-80	M	EGD	Duodenum	Positive	24	0	Severe
*10***	*80-85*	*F*	*EGD*	*Duodenum*	*NA*	*NA*	*NA*	*NA*
11	90-95	F	EGD	Duodenum	Positive	36	0	Severe with EOD
12	50-55	F	Colonoscopy	Ileum	NA	37	31	Mild
13	40-45	M	EGD	Duodenum	Positive	18	0	Mild
14	65-70	F	EGD	Duodenum	Positive	37	32	Severe with EOD
15	30-35	F	EGD	Duodenum	Positive	50	48	Mild
16	70-75	F	EGD	Duodenum	Positive	25	19	Mild
17	50-55	M	EGD	Duodenum	NA	52	52	Mild
18	35-40	M	EGD	Duodenum	NA	3	3	Asymptomatic / mild

* Age is provided as a range to obscure identifying information related to individuals

**Patient 10 was excluded from analysis because SARS-CoV-2 nasopharyngeal PCR testing was repeatedly negative and her COVID-19 antibodies were also negative. Her inclusion initially was based on an atypical pulmonary infiltrate on chest X-ray and a viral syndrome in two of her family members.

Fig. 1: GI symptoms in COVID-19 patients associated with reduced severity and mortality

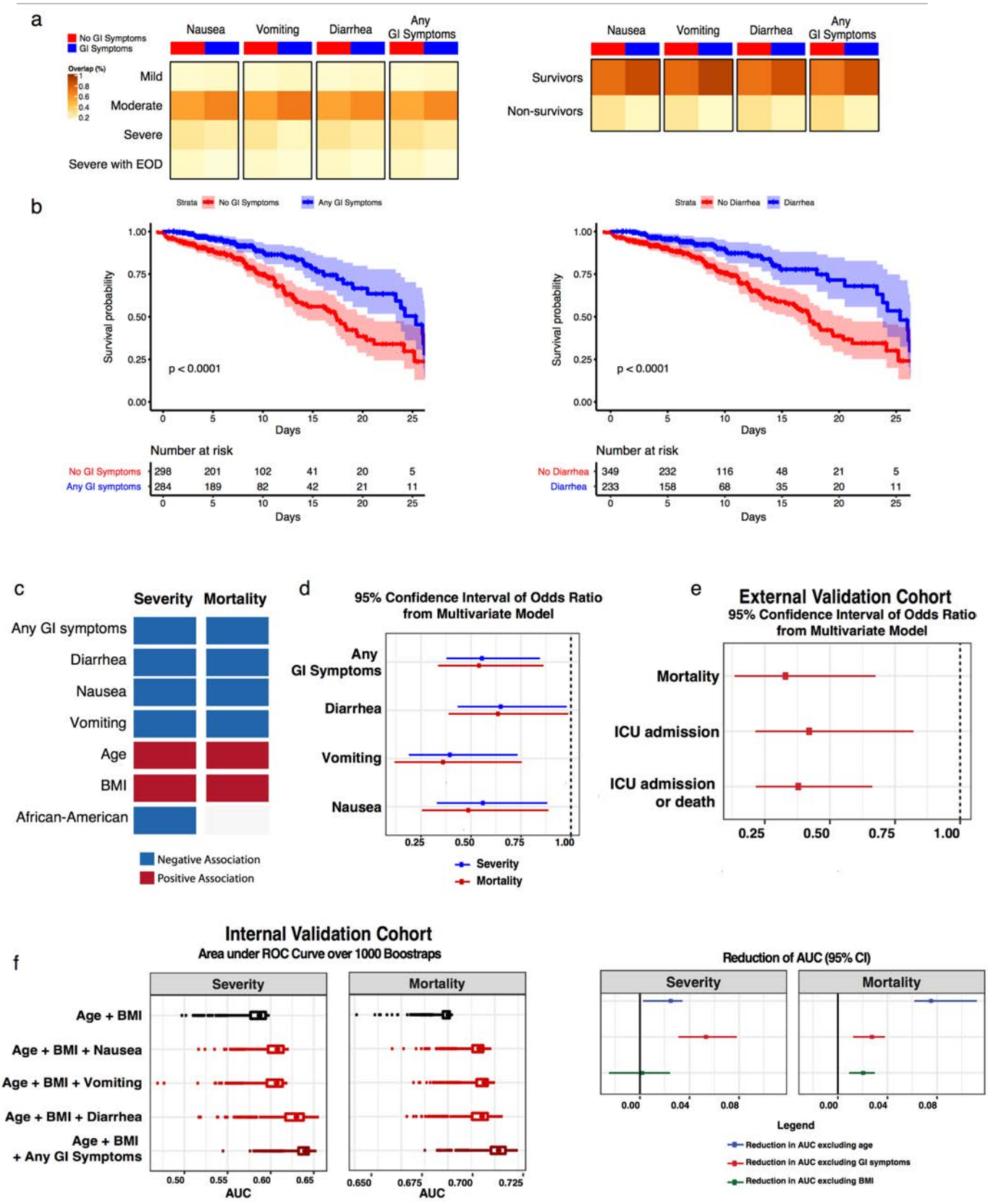

a, Inverse association between GI symptoms (nausea, vomiting, diarrhea, and any GI symptoms) with severity and mortality in the discovery cohort. For each GI symptom (columns), the percentage of patients allocated (as indicated by % overlap) to severity and mortality status (rows) is displayed. P-values from Fisher-Exact test for the association between GI symptoms and severity (less than 0.001) or mortality (less than 0.05). **b,** Kaplan-Meier (KM) curves for survival stratified by any GI Symptoms (left panel) and diarrhea (right panel) for patients in the Discovery Cohort. P-values from log-rank test and 95% confidence intervals of KM curves are shown. Below each KM curve, the number of patients at risk are reported for the respective time points. **c,** Significant variables associated with mortality and severity in multivariate logistic regression. Significant associations were derived via 95% confidence intervals based on 1000 bootstrap iterations. Negative associations are displayed in blue; while positive associations in red. Severity and mortality were modeled as function of each individual GI symptom (i.e., nausea, vomiting and diarrhea) and any GI symptoms, and covariates including age, gender, BMI, hypertension, diabetes, lung and heart diseases. This plot shows the sign of association of each GI symptom and the covariates which were found significant across different GI symptoms models. **d,** Confidence intervals of odds ratio (95%) of GI symptoms based on 1000 bootstrap iterations based on multivariate logistic regression for severity (blue) and mortality (red). **e,** Validation based on the external cohort. Confidence intervals of odds ratio (95%) of diarrhea covariate based on 1000 bootstrap iterations to capture mortality, ICU and composite outcome of ICU admission or death. Results are based on multivariate models after accounting for confounders such as BMI, age, gender, lung disease, heart diseases and hypertension. **f,** Validation and prediction model based on the internal cohort. Boxplot of AUC over 1000 bootstrap iterations to predict Mortality and Severity status in the validation cohort (top panel). Confidence intervals of the reduction in AUC (95%) based on 1000 bootstrap iterations for the model “Age + BMI + Any GI Symptoms” after removing age (blue), GI symptoms (red) and BMI (dark-green).

Fig. 2: COVID-19 patients with GI symptoms have reduced levels of circulating inflammatory cytokines.

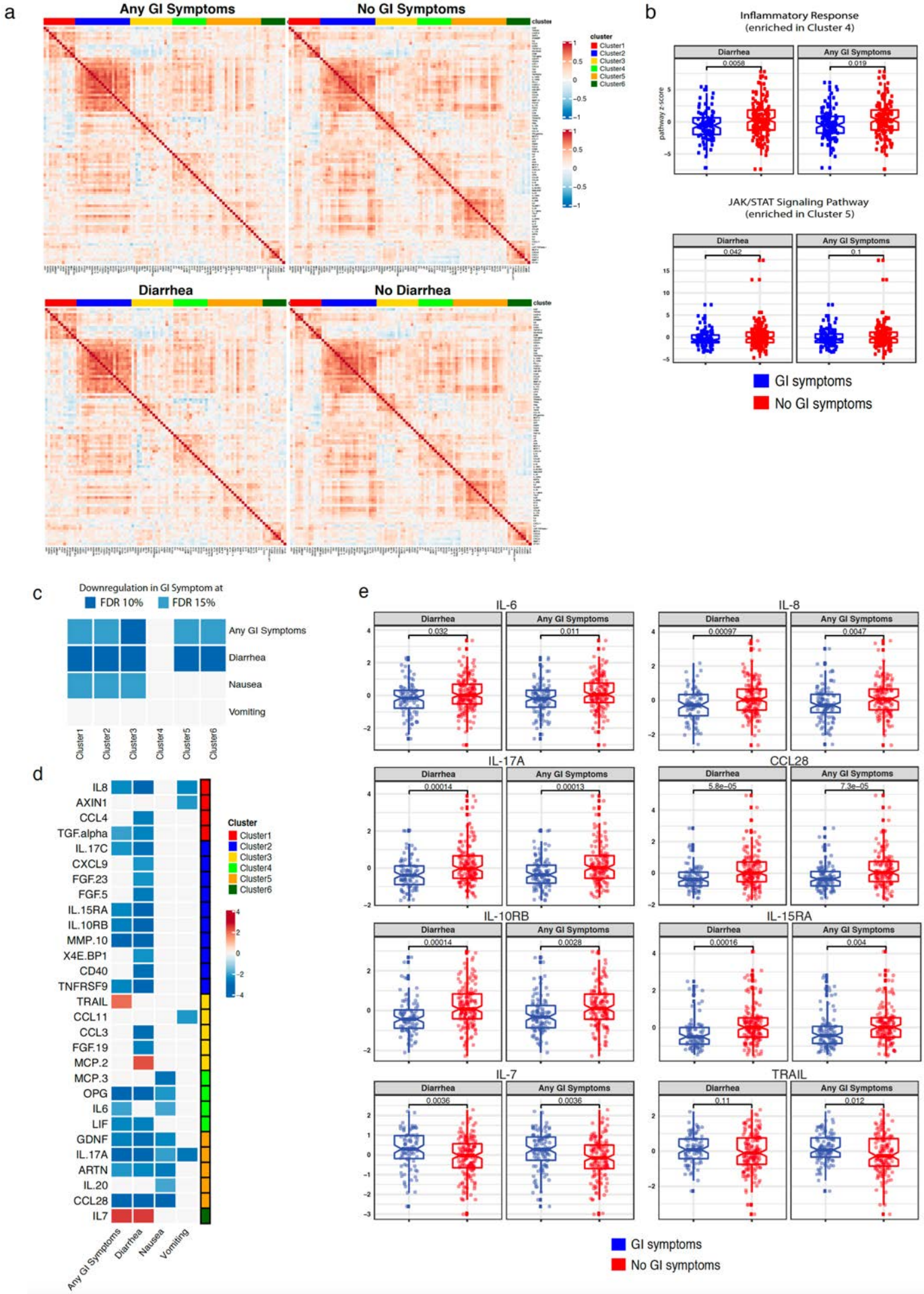

a, Correlation matrix (Pearson's) for 92 markers contained in multiplexed proteomic platform (Olink) across patients with any GI symptoms (top left panel) compared with no GI symptoms (top right panel) and patients with diarrhea (bottom left panel) compared with patients without diarrhea (bottom right panel). Cluster assignment derived based on consensus clustering is reported on the top of the heatmap. **b,** Boxplot of "Hallmark Inflammatory Response" and "KEGG JAK/STAT Signaling pathway" z-scores stratified by GI symptoms. P-values from unpaired t-tests are reported. "Hallmark Immune Response" and "Hallmark JAK/STAT Signaling" pathways were found significantly enriched at 10% FDR in Cluster 4 and Cluster 5, respectively. **c,** Association between proteomic clusters and GI symptoms. This association was derived by comparing clusters signatures between asymptomatic and symptomatic groups via t-test. Associations significant at 10% (dark blue) and 15% (light blue) FDR are reported. **d,** Analytes associated with GI symptoms at 10% FDR based on unpaired t-test. The intensity of the color is proportional to the -log10 p-value. Negative associations are displayed in blue; while positive associations in red. On the right side of the heatmap, the cluster assignment for each marker is reported. **c,** Boxplot of select differentially expressed markers stratified by GI symptoms. P-values from unpaired t-tests are reported.

Fig. 3: Clinical timing and histologic and endoscopic features of COVID-19 in the small intestine.

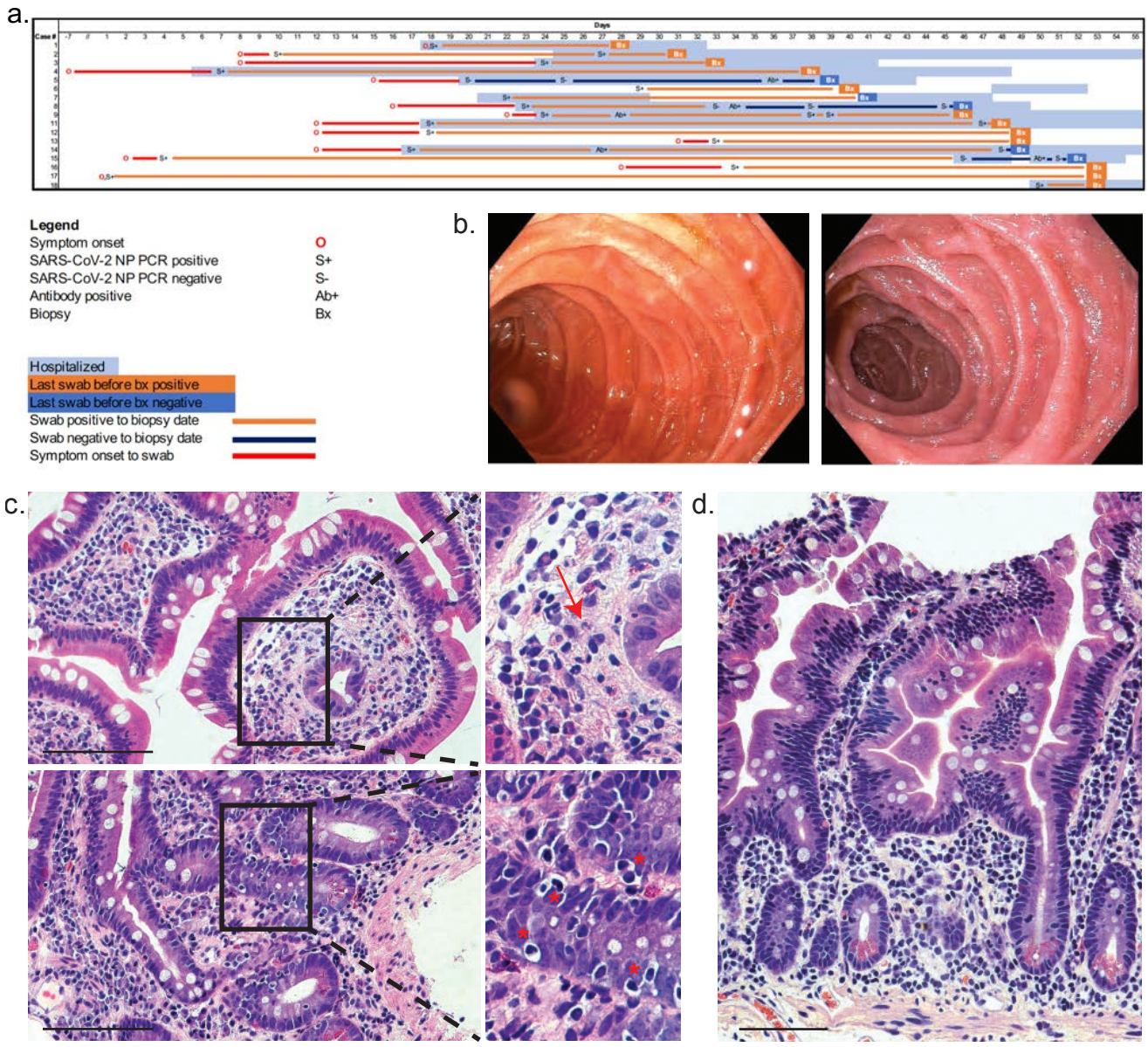

a, Timing of endoscopic evaluation with respect to COVID-19 course. **b,** Representative endoscopic views of the duodenum in COVID-19+ (left) and control (right) subjects. **c,** Histologic signs of inflammation detected in duodenal biopsies of COIVD-19 patients including neutrophils (arrow) and increased intraepithelial lymphocytes (*). **d,** Histologically normal duodenal tissue in a COVID-19 patient. Scale bar; 100 μm.

Fig. 4: SARS-CoV-2 viral particles and protein are detectable in intestinal tissue of COVID-19 patients.

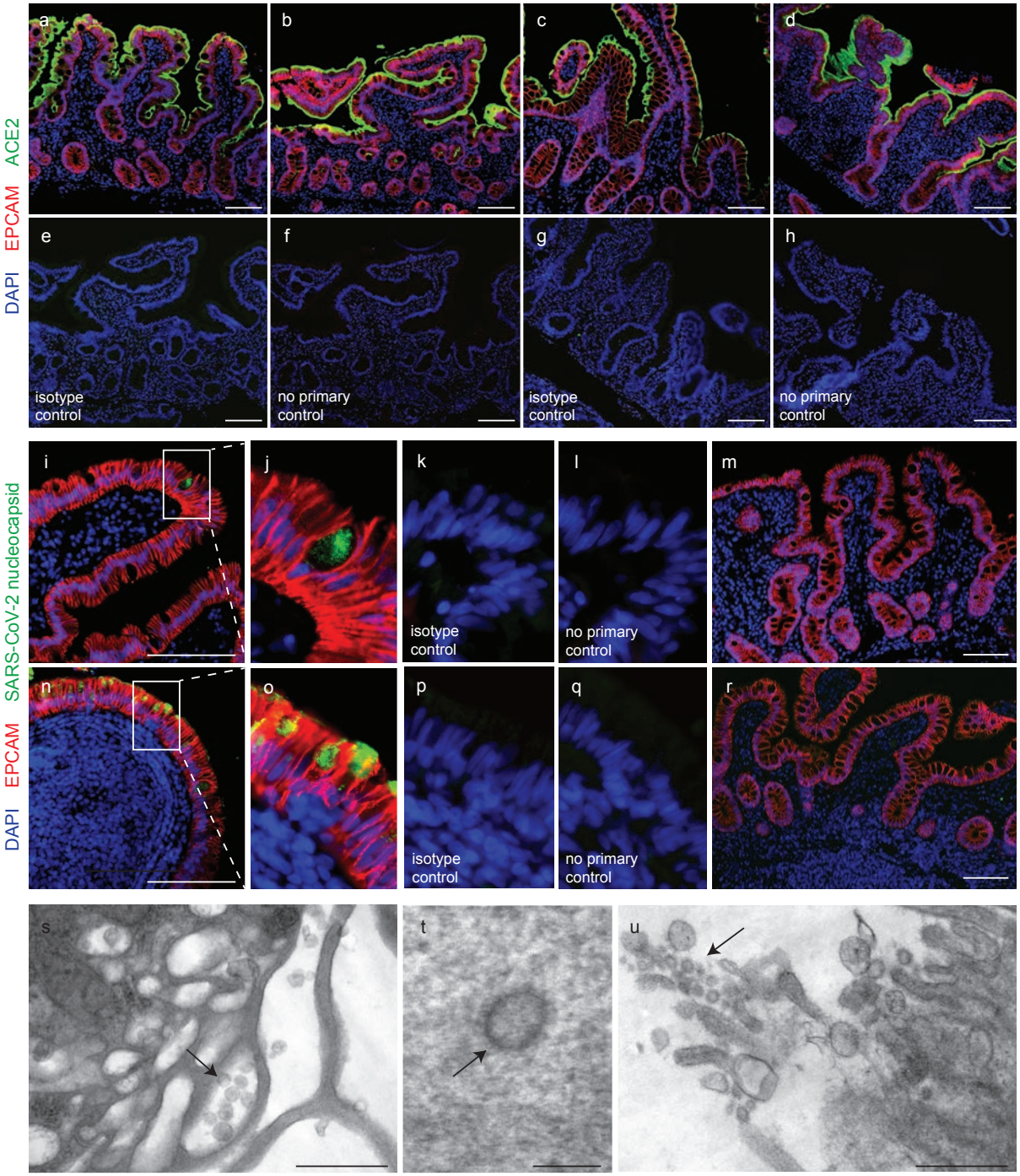

a-h, Immunofluorescent staining of duodenal **(a,b)** and ileal **(c,d)** biopsies of COVID-19 patients **(b,d)** and controls **(a,c)** with ACE2 (green), EPCAM(red) and DAPI (blue) including isotype **(e,g)** and no primary **(f,h)** controls.

i-r, Immunofluorescent staining of duodenal **(i-m)** and ileal **(n-q)** biopsies from COVID-19 patients **(i-l, n-q)** and controls **(m,r)** with SARS-CoV-2 nucleocapsid (green), EPCAM (red) and DAPI (blue) including isotype **(k,p)** and no primary **(j,q)** controls.

s-u, Electron microscopy of duodenal biopsies **(s, t)** and an ileal biopsy **(u)** from COVID-19 patients showing viral particles (arrows). Scale bars; 100 µm **(a-r)**, 0.5 µm **(s,u)**, 0.1 µm **(t)**.

Fig. 5: Identification of immune cell signatures in intestinal biopsies and blood from COVID-19 patients and controls based on mass cytometry.

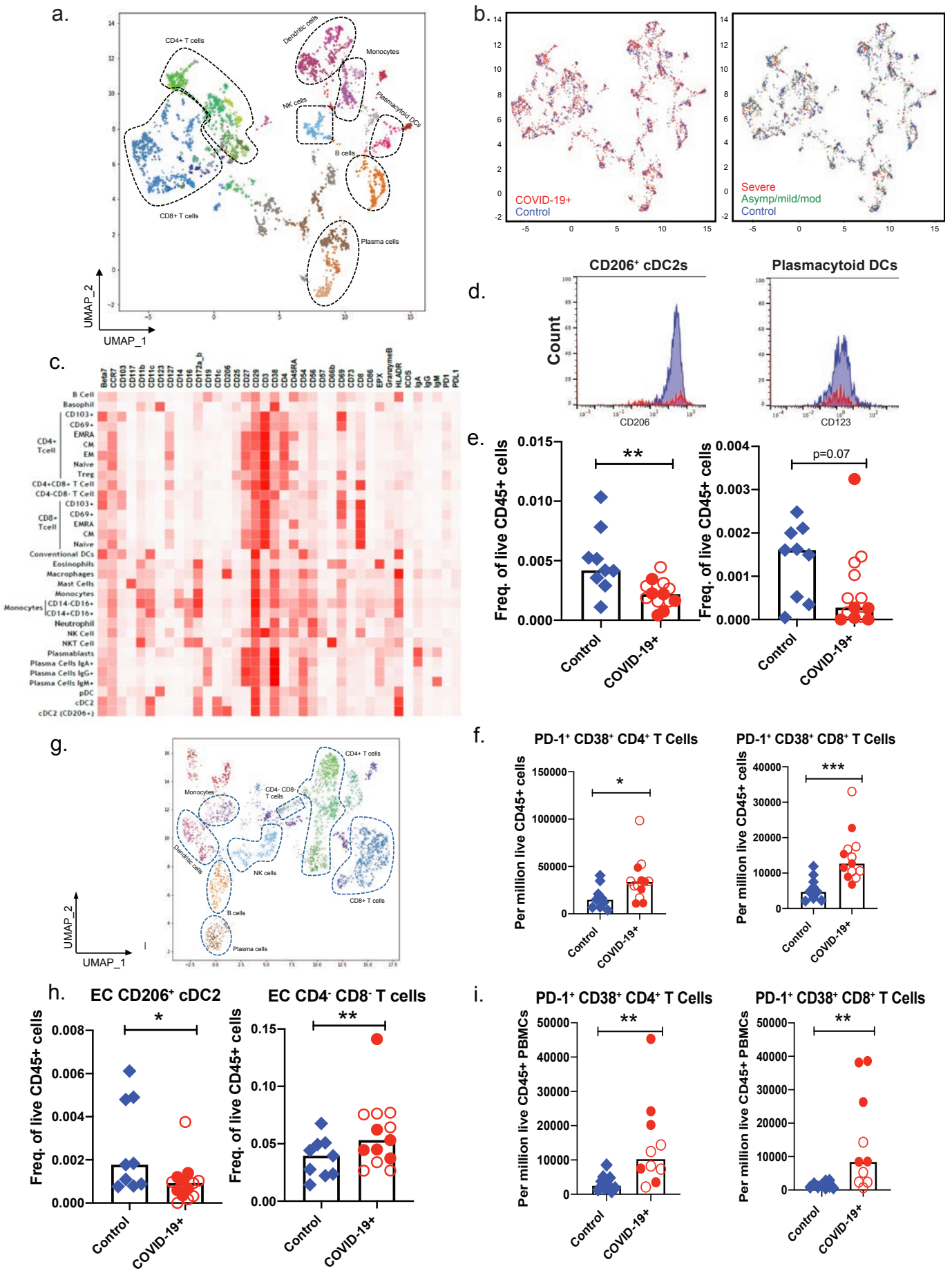

a, Uniform Manifold Approximation and Projection (UMAP) presentation of the eight clusters of immune populations based on 38 markers in lamina propria. **b,** UMAP presentation of clusters defined by COVID-19 (Red) vs Controls (Blue) and clusters defined by cohort where controls are indicated in blue, severe COVID-19 patients indicated in red and asymptomatic/mild/moderate COVID-19 patients are indicated in green in lamina propria. **c,**The heatmap shows the different immune populations based on specific cell type markers in lamina propria of COVID-19 patients and controls. **d,** The histograms shows the decrease in the expression of CD206 and CD123 in dendritic cell populations of COVID-19 patients (red) compared to the controls (blue). **e,** Unsupervised analyses of immune cells: The bar plots show the relative frequencies of different myeloid and lymphocytic immune populations namely CD206+ cDC2 and plasmacytoid DCs in lamina propria of controls (blue) and COVID-19 patients (red).. **f,** Supervised analyses: The bar graphs depict alterations in PD-1+ CD38+ (exhausted) CD4+ and CD8+ T cell subsets in lamina propria of controls (blue) and COVID-19 patients (red). **g,** Uniform manifold approximation and projection (UMAP) presentation of the eight clusters of immune populations based on 38 markers in epithelial compartment of small intestinal biopsies. **h,** Unsupervised analyses of immune cells: The bar plots show the relative frequencies of CD206+ cDC2 dendritic cells and CD4- CD8- T cells in the intraepithelial compartment of controls (blue) and COVID-19 patients (red). **i,** Supervised analyses on PBMCs indicating immune cell changes in blood : The bar graphs depict alterations in PD-1+ CD38+ (exhausted) CD4+ and CD8+ T cell subsets in blood of controls (blue) and COVID-19 patients (red).

Open red circles denote patients with asymptomatic/mild/moderate disease while filled red circles denote patients with severe COVID-19.

Fig. 6: Transcriptional changes in intestinal biopsies from COVID-19 patients against non-infected controls.

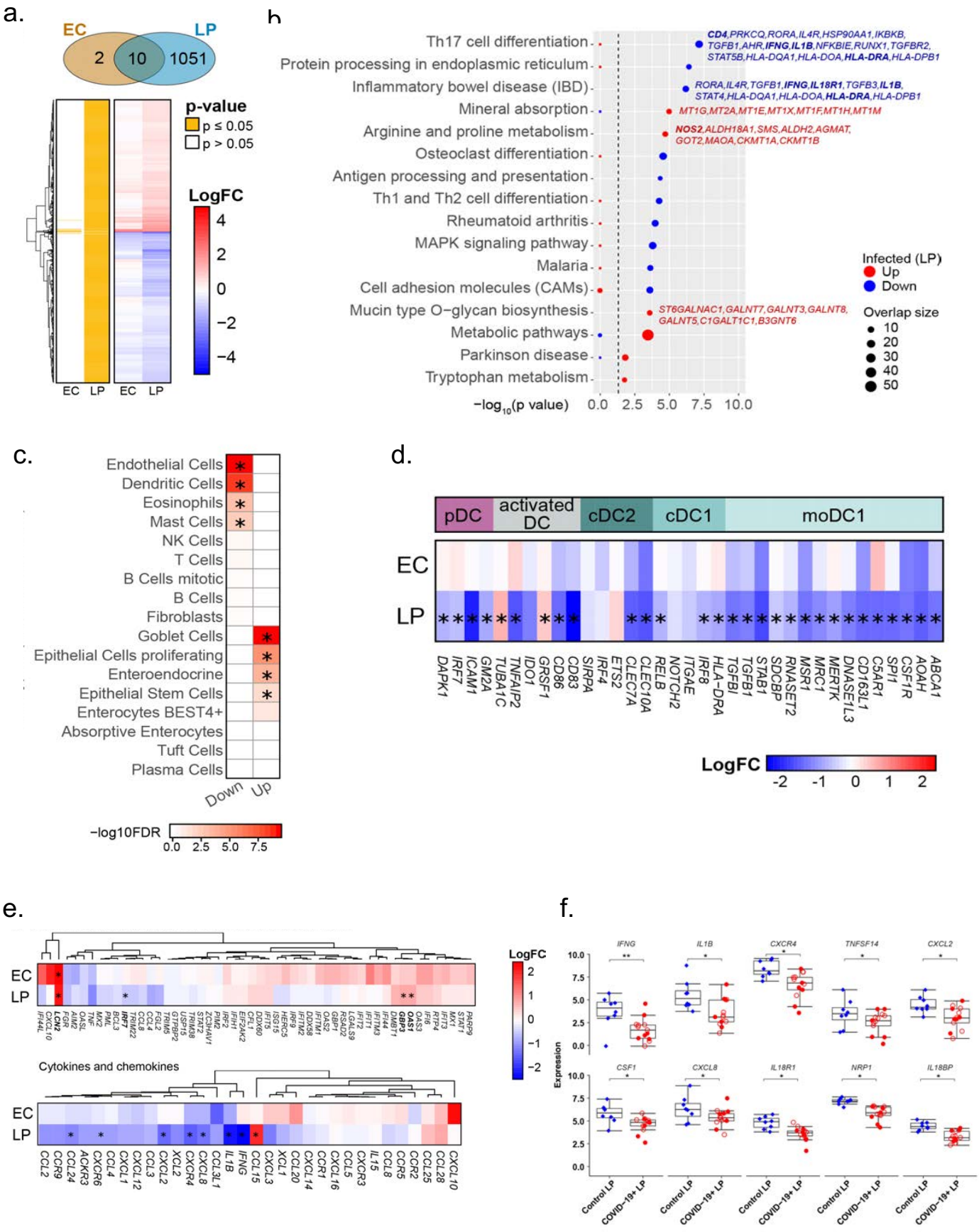

a, Hierarchical clustering of average expression changes for 1,063 genes (rows) with induced (red) or depleted (blue) expression (FDR ≤ 0.05) in the epithelial layer (EC) and lamina propria (LP) sections of intestinal biopsies from COVID-19 patients. The panel on the left indicates significant genes for each tissue section in yellow. The color bar indicates the average log2 fold-change (FC). **b,** Top enriched pathways (KEGG) induced (red) or depleted (blue) in LP. The dash line indicates the p ≤ 0.05 cutoff. Gene names for are indicated for main pathways related to inflammation and cell type composition. The dash line indicates the p ≤ 0.05 cutoff. **c,** Deconvolution of main intestinal (GI) cell types enriched or depleted in the LP section of COVID-19 convalescent patients against controls. Reference scRNA-seq cell type signatures were taken from Smillie et al 2019. (p ≤ 0.05, Fisher's exact test). **d,** Average expression changes for dendritic cell markers in the LP and EC sections. The yellow boxes indicate significant genes for each tissue section. The color bar indicates the average log2 fold-change (FC). **e,** Hierarchical clustering of average expression changes (columns) in the EC and LP sections for genes related to antiviral response to SARS-CoV-2 in post-mortem lung tissue of COVID-19 patients as described by Blanco-Mello et al. 2020 (top panel) and for cytokines and chemokines (bottom panel). Significant genes are indicated by the asterisks. The color bar indicates the average log2 fold-change (FC). **f,** The gene expression levels for the top 10 significant chemokines and cytokines in the LP section of COVID-19 patients (13) and controls (8). $^{*}p < 0.05$, $^{**}p < 0.01$. Open red circles denote patients with asymptomatic/mild/moderate disease while filled red circles denote patients with severe COVID-19.